Characterization of different aspects of selective NCX inhibition in the heart: from inotropy to arrhythmias

Zsófia Nagy, *MSc*
(Birth name: Zsófia Kohajda)

PhD Thesis

Supervisor:
Norbert Jost, *PhD*

Department of Pharmacology and Pharmacotherapy
Faculty of Medicine
University of Szeged
Szeged
Hungary
2017

LIST OF PUBLICATIONS RELATED TO THE SUBJECT OF THE THESIS

Full length papers

I. Kohajda Z, Farkas-Morvay N, Jost N, Nagy N, Geramipour A, Horváth A, Varga RS, Hornyik T, Corici C, Acsai K, Horváth B, Prorok J, Ördög B, Déri Sz, Tóth D, Levijoki J, Pollesello P, Koskelainen T, Otsomaa L, Tóth A, Baczkó I, Leprán I, Nánási PP, Papp JGy, Varró A, Virág L.
The effect of a novel highly selective inhibitor of the sodium/calcium exchanger (NCX) on cardiac arrhythmias in in vitro and in vivo experiments.
PLOS ONE 11(11): e0166041. doi: 10.1371/journal.pone.0166041.eCollection (2016)
IF (2015): 3.057 (Q1)

II. Nagy N, Kormos A, Kohajda Z, Szebeni A, Szepesi J, Pollesello P, Levijoki J, Acsai K, Virag L, Nanasi PP, Papp JGy, Varro A, Toth A
Selective Na^{+}/Ca^{2+} exchanger inhibition prevents Ca^{2+} overload induced triggered arrhythmias.
BRITISH JOURNAL OF PHARMACOLOGY 171(24):pp.5665-5681(2014)
IF: 4.842 (Q1/D1)

III. Jost N, Nagy N, Corici C, Kohajda Zs, Horváth A, Acsai K, Biliczki P, Levijoki J, Pollesello P, Koskelainen T, Otsomaa L, Tóth A, Papp JGy, Varró A, Virág L.
ORM-10103, a novel specific inhibitor of the sodium/calcium exchanger, decreases early and delayed afterdepolarization in the canine heart.
BRITISH JOURNAL OF PHARMACOLOGY 170:(4) pp. 768-778. (2013)
IF: 5.067 (Q1/D1)

Quotable abstracts

Jost N, Zs Kohajda, N Nagy, A Geramipour, RS Varga, T Hornyik, B Horváth, A Kormos, K Acsai, J Levijoki, P Pollesello, T Koskelainen, L Otsomaa, A Tóth, I Baczkó, PP Nánási, JGy Papp, L Virág, A Varró.
Role of Na+/Ca2+ exchanger (NCX) in cardiac automaticity and ventricular repolarization assessed by ORM-10962, a novel highly selective NCX inhibitor
HEART RHYTHM, 13(5S), S6, 2016
IF (2015): 4.391

Nagy N, Kohajda Zs, Acsai K, Kormos A, Tóth A, Oravecz K, Pollesello P, Levijoki J, Virág L, Jost N, Papp JGy, Varró A
Inhibition and activation of the cardiac Na+/Ca2+ exchanger – two aspects of transport modulation
CURRENT RESEARCH: CARDIOLOGY - EXPERIMENTAL CLINICAL 2:(3) p. 143. (2015)

OTHER PAPERS

I. Major P , Baczko I , Hiripi L , Odening KE , Juhasz V , Kohajda Z , Horvath A , Seprenyi G , Kovacs M , Virag L , Jost N , Prorok J , Ordog B , Doleschall Z , Nattel S , Varro A , Bosze Z.
A novel transgenic rabbit model with reduced repolarization reserve: long QT syndrome caused by a dominant-negative mutation of KCNE1 gene.
BRITISH JOURNAL OF PHARMACOLOGY 173:(12) pp. 2046-2061. (2016)
IF: 5.259 (Q1/D1)

II. Ordog B , Hategan L , Kovacs M , Seprenyi G , Kohajda Z , Nagy I , Hegedus Z , Kornyei L , Jost N , Katona M , Szekeres M , Forster T , Papp JG , Varro A , Sepp R
Identification and functional characterisation of a novel KCNJ2 mutation, Val302del, causing Andersen-Tawil syndrome
CANADIAN JOURNAL OF PHYSIOLOGY AND PHARMACOLOGY 93:(7) pp. 569-575. (2015) IF: 1.704 (Q2)

III. Corici C , Kohajda Z , Kristóf A , Horvath A , Virág L , Szél T , Nagy N , Szakonyi Zs , Fülöp F , Muntean DM , Varró A , Jost N
L-364,373 (R-L3) enantiomers have opposite modulating effects on I-Ks in mammalian ventricular myocytes
CANADIAN JOURNAL OF PHYSIOLOGY AND PHARMACOLOGY 91:(8) pp. 586-592. (2013) IF: 1.546 (Q2)

IV. Jost N , Virág L , Comtois P , Ördög B , Szűts V , Seprényi Gy , Bitay M , Kohajda Zs , Koncz I , Nagy N , Szél T , Magyar J , Kovács M , Puskás LG , Lengyel Cs , Wettwer E , Ravens U , Nánási PP , Papp JGy , Varró A , Nattel S
Ionic mechanisms limiting cardiac repolarization-reserve in humans compared to dogs.
JOURNAL OF PHYSIOLOGY-LONDON 591:(17) pp. 4189-4206. (2013)
IF: 4.380 (Q1/D1)

V. Kristóf A , Husti Z , Koncz I , Kohajda Zs , Szél T , Juhász V , Biliczki P , Jost N , Baczkó I , Papp JGy , Varró A , Virág L
Diclofenac prolongs repolarization in ventricular muscle with impaired repolarization reserve.
PLOS ONE 7:(12) p. e53255. (2012)
IF: 3.730 (Q1)

VI. Jost N , Kohajda Z , Kristof A , Kovacs PP , Husti Z , Juhasz V , Kiss L , Varro A , Virag L , Baczko I
Atrial remodeling and novel pharmacological strategies for antiarrhythmic therapy in atrial fibrillation.
CURRENT MEDICINAL CHEMISTRY 18:(24) pp. 3675-3694. (2011)
IF: 4.859 (Q1)

VII. Virág L , Jost N , Papp R , Koncz I , Kristóf A , Kohajda Zs , Harmati G , Carbonell-Pascuall B , Ferrero JM , Papp JGy , Nánási PP , Varró A
Analysis of the contribution of I(to) to repolarization in canine ventricular myocardium.
BRITISH JOURNAL OF PHARMACOLOGY 164:(1) pp. 93-105. (2011)
IF: 4.409 (Q1/D1)

TABLE OF CONTENTS

ACRONYMS AND ABREVIATIONS

AP: action potential
APD: action potential duration
APD_{90}, APD_{75}, $APD_{50,}$ APD_{25}: action potential durations at 90%, 75%, 50% and 25% of repolarization
ATP: adenosine-triphosphate
ATX-II: anemone toxin
AU: arbitrary unit
CICR: Ca^{2+} induced Ca^{2+} release
CaT: Ca^{2+} transient
dV/dtmax: maximum rate of depolarization
DAD: delayed afterdepolarisation
DD: diastolic depolarization
DMSO: dimethyl sulfoxide
EAD: early afterdepolarisation
ECC: excitation-contraction coupling
FSK: forskolin
$[Ca^{2+}]i$: intracellular Ca^{2+}
I_f: pacemaker or “funny” current
I_{CaL}: L-type Ca^{2+} current
I_{CaT}: T-type Ca^{2+} current
I_{K1}: inward rectifier K^+ current
I_{Kr}: rapid component of the delayed rectifier K^+ current
I_{Ks}: slow component of the delayed rectifier K^+ current
I_{Na}: Na^+ current
I_{NaL}: Late Na^+ current
I_p: Na^+/K^+ pump current
$I_{Na\ peak}$: peak Na^+ current
I_{to}: transient outward K^+ current
M cells: midmyocardial cells
MDP: maximum diastolic potential
NCX: Na^+/Ca^{2+} exchanger
PLB: phospholamban
PMCA : sarcolemmal Ca^{2+} ATPase
$Plateau_{50}$: plateau potential at 50% repolarization time
RyR: ryanodine receptor
SA node, SAN: sinoatrial node
SERCA2a: myocardial sarcoplasmic reticulum Ca^{2+} ATPase
SR: sarcoplasmic reticulum
Vmax: maximum rate of depolarization

SUMMARY

The cardiac sodium-calcium exchanger (NCX) has a pivotal role in the Ca^{2+} homeostasis as well as in several types of arrhythmias; therefore the potential therapeutic application of its modification was intensively studied in the past decade. However, the inotropic and antiarrhythmic effect of its inhibition has not yet been fully clarified due to the lack of appropriately selective inhibitor. The recently developed novel selective NCX inhibitors, ORM-10103 and especially ORM-10962, provided new insights in the understanding of NCX physiology as well as the possible therapeutic implications of these new potential drugs as novel antiarrhythmic agents.

This thesis summarizes:

1) The pharmacological profile of the novel NCX inhibitor ORM-10962, compared its selectivity with that of the previously described compound, ORM-10103. ORM-10962 proved to be even more selective and exerts improved effectiveness on NCX current having EC_{50} values in the nanomolar range, without any influence on I_{CaL} or other currents.
2) In contrast to previous inhibitors like SEA0400 or ORM-10103, we found marginal positive inotropic effect of the ORM-10962 without major influence on the action potential under normal condition.
3) Marginal but statistically significant reduction by ORM-10962 in the spontaneous firing rate of the atrial and Purkinje AP may indicate important role of NCX in the spontaneous pacemaker mechanism, which is in the line with the previously described coupled clock hypothesis.
4) We suggest that NCX inhibition could equally lead to positive and negative inotropy, depending on the actual value of NCX reversal potential. Selective NCX inhibition may have negative inotropic effect when Ca^{2+} load is coupled with marked increase of intracellular Na^{+} facilitating the reverse mode activity. This hypothesis was tested in dog Purkinje fibres, where digoxin induced DADs amplitude and incidence were significantly reduced by ORM-10962.

1. INTRODUCTION

1.1. The cardiac action potential and its underlying currents

The normal mechanical (pump) function of the mammalian heart depends on proper electrical function, as reflected in the successive activation of cells in specialized, "pacemaker" regions of the heart and the propagation of activity through the ventricles. Myocardial electrical activity is attributed to the generation of action potentials (AP) in individual cardiac cells, and the normal coordinated electrical functioning of the whole heart is readily detected in surface electrocardiograms (1). The generation of myocardial APs reflects the consecutive activation and inactivation of ion channels that conduct depolarizing, inward (Na^+ and Ca^{2+}), and repolarizing, outward (K^+), currents. The waveforms of APs in different regions of the heart show some variances reflecting to differences in the expression and/or the properties of the underlying ion channels. These differences contribute to the normal unidirectional propagation of excitation through the myocardium and to the generation of normal cardiac rhythms (2, 3). The cardiac electrical cycle has been divided into five “phases”, four of them describing the AP contour and one the diastolic interval (**Figure 1.**). The initial phase (*phase 0*) refers to the fast depolarization of the AP supported by the activation of fast inward Na^+ channels. However, this current (I_{Na}) has relatively short-lived characteristic (activation time of the fast current is no longer than 2-3 ms), provides large enough charge influx to membrane depolarization. Beyond activating other currents of the AP (e.g.: Ca^{2+}-current, K^+-currents) this phase is responsible for the rapid impulse propagation. The *phase 1* reflects a transient repolarization, mainly supported by transient outward potassium current (I_{to}). The kinetics of this current is similar to the I_{Na}, it is quickly activated and inactivated during depolarization. The magnitude of this phase has important role in shaping the spike-and-dome configuration of the AP. Since the expression level of ion channel(s) carrying I_{to} exerts marked differences across the ventricular wall (and therefore the amplitude of I_{to} as well) (4) the spike-and-dome configuration can be considered a specific “marker” in identifying the ventricular origin of the cell. The *phase 2* also named “plateau phase”, which is a characteristic feature of the cardiac AP. During this phase the inward and outward currents transiently balance each other, providing a long-lasting isoelectric phase, which has crucial role in cell contraction. Thus I_{CaL} is an important player not only in shaping the action potential, but in initiation of intracellular Ca^{2+} cycle (see details in chapter 1.2). When I_{CaL} slowly decays, the outward K^+-currents overcome the charge influx, allowing

repolarization (*phase 3*). During the initial section of phase 3, the rapid and slow components of delayed rectifiers (I_{Kr} and I_{Ks}) support large outward K^+-current having crucial role in repolarization, while in the terminal phase of the AP, the inward rectifier K^+ current (I_{K1}) has primary function in the complete repolarization. The *phase 4* represents the resting membrane potential during diastole. Mainly I_{K1} and perhaps the Na^+/K^+ pump has important role in maintaining the stable resting membrane potential in ventricular cells. In atrial and Purkinje cells, where the expression level of I_{K1} is significantly smaller (5, 6), the resting membrane potential is unstable, and a slow depolarization can be observable (diastolic depolarization), which has important role in the pacemaker function.

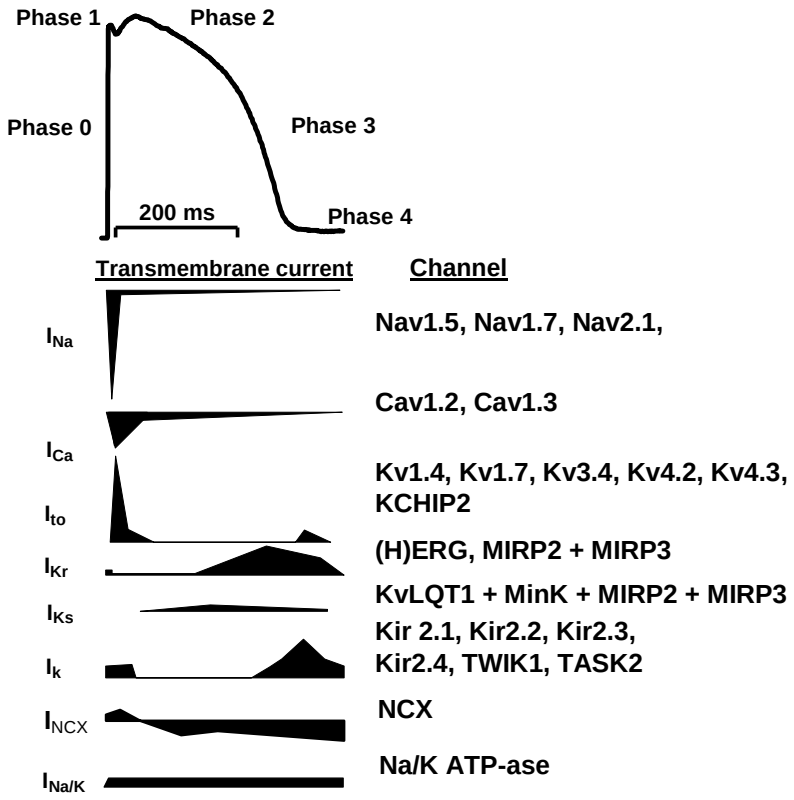

Figure 1. The ventricular action potential and corresponding ion currents. *The upper panel shows a representative ventricular AP and phases of the AP kinetics. The underlying ionic currents are shown in the left side of the lower panel in time-match with the AP. The inward currents are depicted as downward deflections. Note that the amplitudes of the currents are not proportional with each other. The channel proteins carrying the current are marked at right side of the lower panel (modified from (7))*

1.1.1. The concept and role of the repolarization reserve

The concept of the repolarization reserve was introduced by Roden, based on clinical observations (8). The phase 3 of the AP is controlled by a precise cooperation of several

potassium currents including I_{Kr}, I_{Ks} and I_{K1} and I_{to} currents (9, 10). Based on clinical (8) and experimental observation (9-11) it was concluded that in the mammalian (human, dog and rabbit) ventricular muscle, inhibition of one type of potassium channels does not cause excessive APD lengthening. This is probably due to the capability of the various potassium channels which are able to substitute and/or supplement each other. Human, dog and rabbit ventricular myocytes seem to repolarize with a strong safety margin ("repolarization reserve"). This repolarization capacity has important role in decreasing the transmural APD dispersion, thus in preventing life-treating arrhythmias. When this normal repolarization reserve is attenuated due to drug exposures (cardiac and non-cardiac drugs as well), remodelling caused by diseases (heart failure, diabetes mellitus, hypothyroidism, etc), increased sympathetic activity, extreme bradycardia, hypokalaemia or genetic disorders (long QT syndromes, Brugada, etc), the otherwise minimal or moderate potassium current inhibition can result in excessive and potentially proarrhythmic prolongation of the ventricular action potential duration. Multiple K^+ channel block can result in excessive repolarization lengthening by eliminating the repolarization reserve and therefore it can be associated with increased proarrhythmic risk.

1.1.2. Transmural heterogeneity in the ventricular myocardium

Studies described important electrophysiological and pharmacological regional differences of ventricular myocardium in mammalian heart (4). We can distinguish four functional cell types in the ventricles: epicardial, midmyocardial, endocardial and Purkinje cells. Epicardial and endocardial cells have shorter AP than midmyocardial cells. In epicardium the I_{to} and I_{Ks} are more abundantly expressed than in other layers. Midmyocardial cells (M cells) have intermediate electrophysiological features compared with Purkinje cells and its pharmacological responses are different from those of either epicardium or endocardium. Compared with the epicardium and endocardium, the M cells can be characterized by lowest I_{Ks} and highest I_{NaL} expression levels, pronounced frequency dependence of the APD, and marked effect of potassium inhibitions on repolarization (12, 13). The M cells are well coupled electrically with the epicardium and endocardium to stabilize and compensate for the extreme APD lengthening. The I_{CaL}, I_{Kr} and I_{K1} are similar in the cardiac layers, but sodium/calcium exchanger (NCX) may exhibit the most abundant expression level in M cells (14).

1.2. Structure and function of the sodium/calcium exchanger in the heart

Mammalian Na^+/Ca^{2+} exchangers (NCX) are members of a large Ca^{2+}/CA superfamily, whose primary role is to control transmembrane Ca^{2+}-fluxes. Three isoforms of NCX exist (NCX1, NCX2, NXC3), but NCX1 is the only isoform expressed in the heart. NCX1 is a plasma membrane protein, having 10 transmembrane segments (TMS) and assembled as a dimer (15, 16). Between the TMSs 5 and 6 is a large cytoplasmic loop playing regulatory role. This loop contains two Ca^{2+} binding domains, CBD1 and CBD2. When extracellular Ca^{2+} is high, Ca^{2+} binds to the CBD domains and increases the channel activity *via* allosteric activation. In cardiac myocytes, NCX is located mostly at the T-tubules (17-19).

1.2.1. Physiological role of NCX in ventricular myocardium

NCX is an important contributor to the Ca^{2+} homeostasis in the myocardium, having a crucial role in Ca^{2+} extrusion from the cell. The NCX is tightly regulated by the transmembrane Na^+ and Ca^{2+} gradients and by the actual level of the membrane potential.

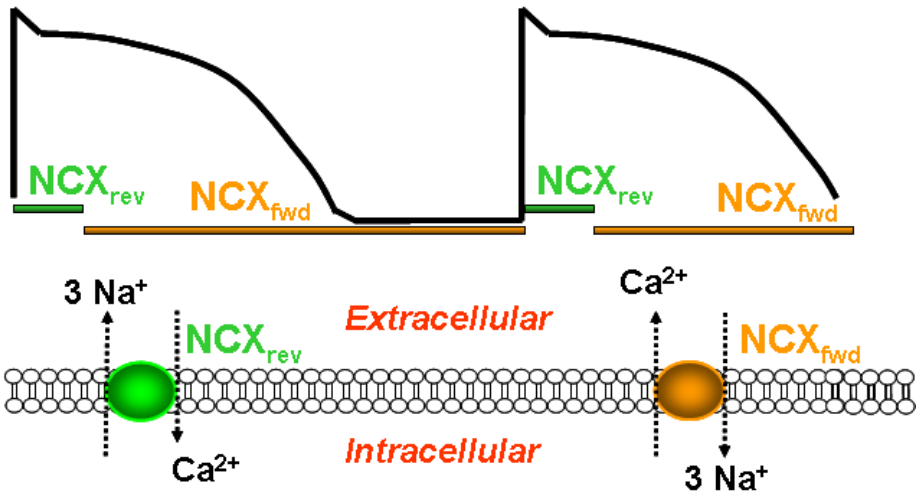

Figure 2. Schematic presentation of two modes of NCX current under action potential. *The reverse mode of the NCX (labelled with green) is only present in the early phase of the AP, when NCX extrudes 3 Na^+ from the cell and moving Ca^{2+} into the cell making an outward current. The forward mode NCX operates during most of the AP (labelled with orange), when Ca^{2+} extrusion is coupled with 3 Na^+ ion entering to the cell, making an inward current.*

NCX can operate in a bidirectional fashion (**Figure 2.**). In the forward mode NCX extrudes 1 Ca^{2+} from the cell which is coupled with 3 Na^+ ions entering the cell. Thus, the forward mode generates inward current, which eventually depolarizes the cell membrane. The reverse mode of the NCX is activated when the cytoplasmic Na^+ level is increased and the

Ca^{2+} concentration is low and/or the membrane potential is depolarized. In this mode the NCX extrudes 3 Na^{+} from the cell and moving 1 Ca^{2+} into the cell, and it can generate repolarizing net current. Under physiologic conditions, NCX operates mainly in forward mode and removes the same amount of Ca^{2+} that entered the cell through I_{CaL} maintaining the beat-to-beat Ca^{2+} balance. In the same time, Ca^{2+} elimination leads to Na^{+} influx (20).

Figure 3 summarizes the Ca^{2+} handling in the cardiac myocardial cell. In the excitation-contraction coupling (ECC), Ca^{2+} ions enter the cell from the extracellular space (Ca^{2+}-influx) mainly *via* I_{CaL}. These channels are primarily present at sarcolemmal - sarcoplasmatic reticulum (SR) junctions, in the vicinity of ryanodine receptors (RyRs). The Ca^{2+} influx increases the Ca^{2+} concentrations near the RyRs, which triggers Ca^{2+} release from the sarcoplasmic reticulum (SR). This mechanism is called 'Ca^{2+}-induced Ca^{2+} release' (CICR), which leads more Ca^{2+} to be released into the cytosol, resulting in a Ca^{2+} transient (CaT). In cardiac muscle CaTs can be observed as a summary of spatio-temporally restricted Ca^{2+} sparks, which can be monitored by optical (fluorometric) techniques. The free intracellular Ca^{2+} binds to the myofilaments and triggers contraction. After the contraction the released $[Ca^{2+}]_i$ is eliminated by both Ca^{2+} reuptake to the SR *via* the activity of the SR Ca^{2+} pump (SERCA2a), and Ca^{2+} extrusion (efflux) from the cell (primarily by the forward mode activity of the NCX) (21-23).

Sequestration of the released Ca^{2+} and stabilization of the diastolic $[Ca^{2+}]_i$ between contractions is crucial in the regulation of the beat-to-beat Ca^{2+} balance under varying conditions. The majority of the released Ca^{2+} is reuptake by SERCA2a. A much smaller amount of $[Ca^{2+}]_i$ is extruded from the cell, primarily *via* the forward mode activity of the NCX. An ATP-dependent Ca^{2+} transporter, the Ca^{2+} pump of the plasma membrane (PMCA) may also extrudes Ca^{2+}, however its contribution to maintaining Ca^{2+} balance is much less important, and its role is suggested to be primarily restricted to fine tuning of the diastolic Ca^{2+} level (24). In steady state, during each cycle, the released and reuptake Ca^{2+}, as well as the entered and extruded Ca^{2+} must be equal.

In the past two decades, several NCX inhibitors were developed having different potency and selectivity. The KB-R7943 markedly suppressed the NCX current however exerted poor selectivity (25). The SEA0400 is a widely used, potent NCX inhibitor which considerably improved our knowledge about the NCX function however a ~ 20% inhibition of I_{CaL} made the data interpretation difficult (25). The ORM-10103 (10) and ORM-10962 (26) are recently synthesised, novel NCX inhibitors having an appropriate selectivity profile to investigate the NCX function (for details see the chapter 1.3).

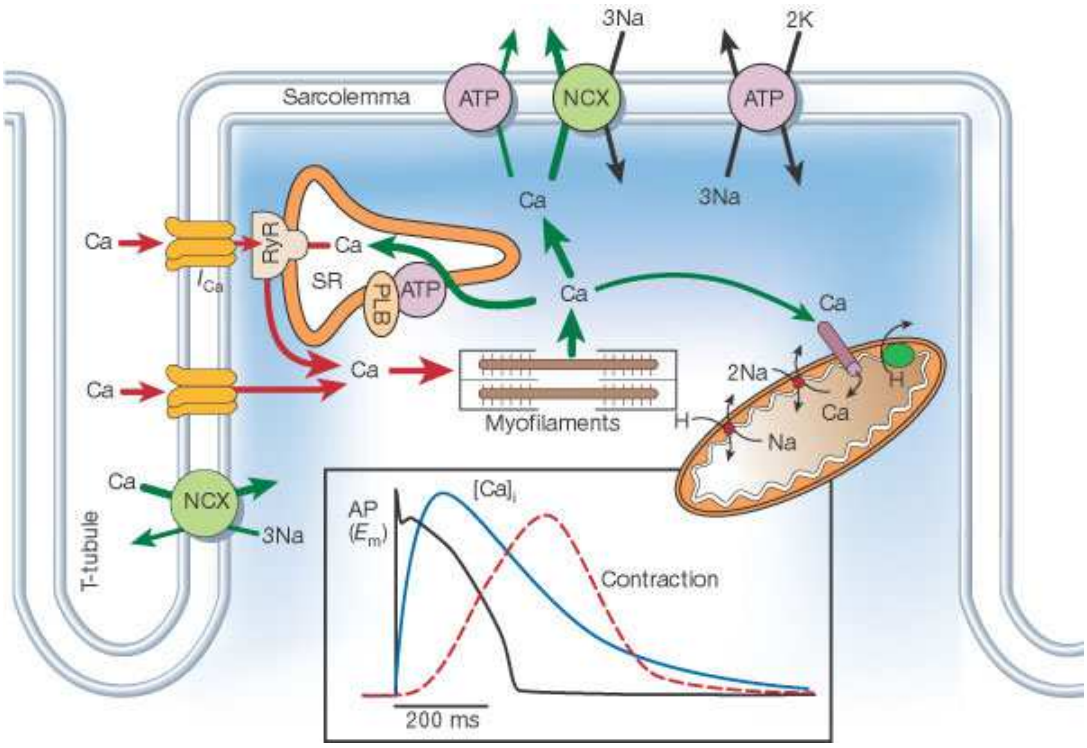

Figure 3. Intracellular Ca^{2+} homeostasis of the cardiac cell. *The upper panel shows the main routes of the Ca^{2+} movements of the cell, the inset shows the time course of an action potential, Ca^{2+} transient and contraction. NCX; Na^+ /Ca^{2+} exchange; ATP, ATPase; PLB, phospholamban; RyR, ryanodine receptors; SR, sarcoplasmic reticulum (21).*

Theoretically (27, 28), the inhibition of NCX may lead to net gain of the intracellular Ca^{2+} and causes positive inotropy. This effect may have important clinical implication since during heart failure (HF), the Ca^{2+}content of the cells is decreased thus the pump function is reduced. However, the possible positive inotropic effect of selective NCX inhibition remained controversial in the literature. Studies performed on rat myocytes and Langendorff perfused heart experiments (29, 30) reported clear positive inotropic effect of SEA-0400 however SEA0400 and ORM-10103 failed to influence the Ca^{2+} transients in dog ventricular cells (28, 31, 32). The controversial results may be caused by the incomplete selectivity of the applied drugs and/or interspecies differences, especially in the kinetics of the action potentials and the intracellular ion levels of the cells.

1.2.2. Possible role of NCX in the pacemaker tissue

The sinoatrial node (SA node) is the primary pacemaker in the heart generating regular, spontaneous APs, to initiate the normal cardiac cycle. Pacemaker potentials are often referred as "slow response" action potentials suggesting relatively low kinetics of the I_{CaT} (transient or T-type Ca^{2+} current) and I_{CaL} during depolarization. The upstroke of the AP is

preceded by a slow diastolic depolarization (DD), which slowly depolarizes the membrane potential to reach the excitation threshold. SA nodal AP can be divided into three phases (**Figure 4. top**). *Phase 4* is the DD, which triggers the AP, when membrane potential reaches the threshold (between -30 and -40 mV). Initiator current is the hyperpolarization activated, so called "funny current" (I_f), which carries slow inward Na^+ current. When the membrane potential reaches ~ -50 mV I_{CaT} is activated and the Ca^{2+} influx mediated additional depolarization activates I_{CaL}. *Phase 0* is the depolarization phase of the AP and primarily caused by increased Ca^{2+} conductance (gCa^{2+}) through I_{CaL} channels. This is followed by *phase 2* repolarization, by outward K^+ currents. While the conductance (g) of the calcium channels decreasing by inactivation of I_{CaL}, the gK^+ is increasing and hyperpolarizes the cell membrane. I_{K1} is not expressed or it is very small in some species in these regions, so the maximum diastolic potential (MDP) in is about -65mV, which is higher than the resting potential, ~ -90mV in ventricular myocytes. Any impact which changes the slope of DD will have an effect on cycle length and heart frequency. Under sympathetic stimulus and in hypokalaemia the slope of DD is increasing and enhances the automaticity, however, under increased vagal tone the slope of DD is decreasing, causing reduced spontaneous AP firing rate. Recent works in the atrioventricular node and Purkinje cells suggest that the mechanisms governing sino-atrial node automaticity are likely to be similar in all pacemaking tissues (33, 34).

During spontaneous pacemaking, several ion channels (I_f, I_{CaT}, I_{CaL}, I_K) with finely tuned kinetics cooperate during an AP waveform, this collective behaviour has been termed as "the membrane clock" (M clock). Dynamic time- and voltage-dependent interaction of the above membrane-limited electrogenic ion channels leads DD from MDP to threshold potential. M clock interacting with the intracellular Ca^{2+} cycling transport mechanism establishes the "Ca^{2+} clock". The main phenomenon is the spontaneous, periodic local subsarcolemmal Ca^{2+} release (LCRs) from SR during DD in pacemaker cells. These 1-5Hz LCRs activate NCX forward mode, and Ca^{2+} extrusion due to Na^+ influx making a depolarizing current. This current may accelerate the DD and contribute to spontaneous pacemaking. The two clocks may work synergistically forming a coupled-clock system (**Figure 4. bottom**) (35-37).

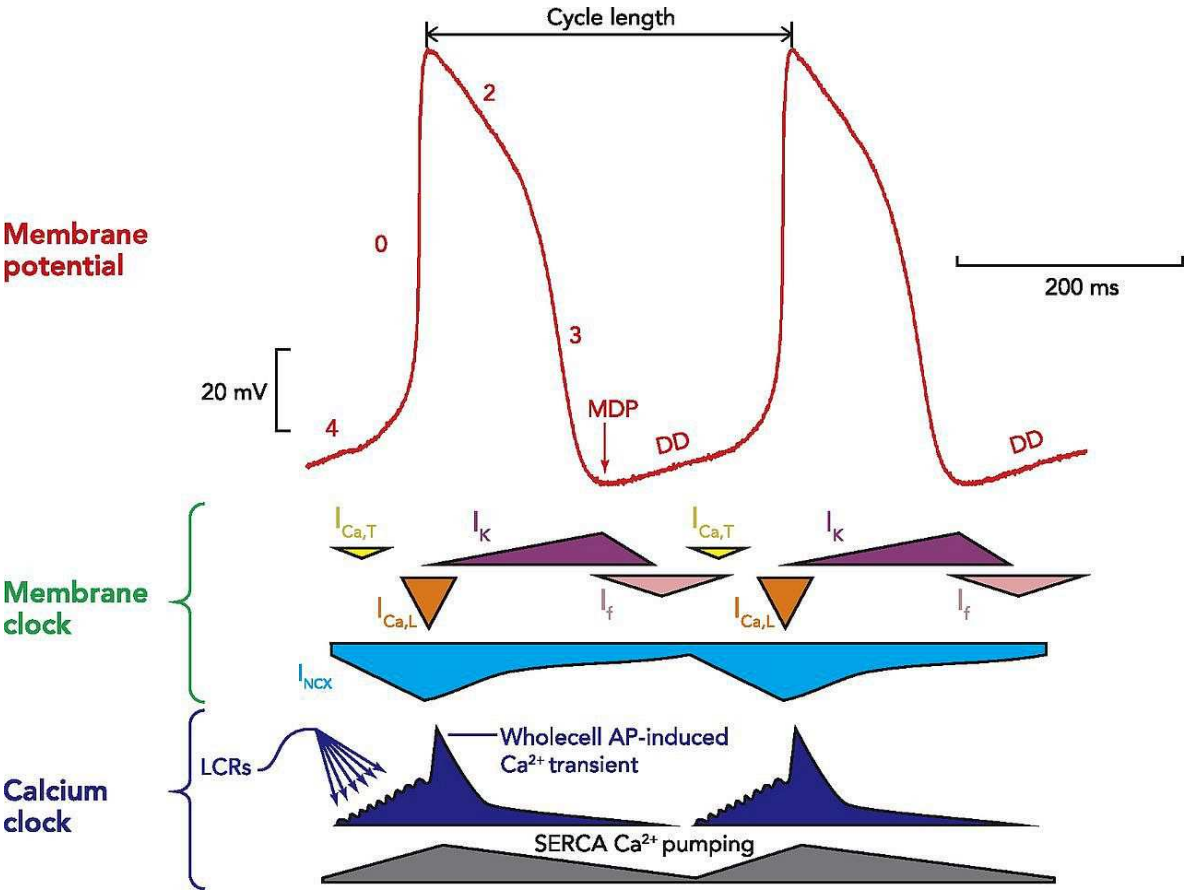

Figure 4. Schematic figure of the pacemaker mechanism of sinoatrial node. *Red trace in the top, represents a typical AP of spontaneously beating nodal cells. The numbers indicate the different phases of the AP. Components of the „membrane clock" are depicted in the middle, components of the "Ca^{2+} clock" are shown in the bottom. (MDP, maximum diastolic potential; DD, diastolic depolarization; I_{CaT}, T-type voltage-dependent Ca^{2+} current; I_{CaL}, L-type voltage-dependent Ca^{2+} current; I_{NCX}, sodium-calcium exchange current; I_K, delayed rectifier potassium current; I_f, funny current; SERCA, sarcoplasmic reticulum ATPase; LCRs, local Ca^{+2} releases (38).*

Previous studies suggested the pivotal role of the NCX in normal automaticity. The low-sodium containing bath solution inhibited spontaneous AP firing in guinea-pig SA node cells via suppressing normal function of NCX (39). Other study reported that depletion of SR store by application of ryanodine markedly disturbed the normal pacemaker activity in rabbit SA node cells (40). However, these interventions may have effects on I_f and I_{CaL} directly, which makes the interpretation difficult. Mouse genetic models revealed that partial atrial NCX1 knock out (~ 90%) caused severe bradycardia and other rhythm disorders (41), while complete atrial NCX knock-out completely suppressed the atrial depolarization exerting ventricular escape rhythm on the ECG (42). The application of KB-R7943, a non-selective NCX inhibitor, also suppressed spontaneous beating in guinea-pig SA node cells (39); however, it has also effect on the Ca^{2+}-currents. The supposed crucial role of NCX in the

normal pacemaker function of SA node cells could not be directly challenged experimentally so far, by the lack of selective NCX inhibitor.

1.2.3. Pathophysiological role of NCX in Na^+ induced Ca^{2+}load

The actual function of the NCX is tightly regulated by the intracellular levels of the Na^+ and Ca^{2+} ions. Therefore, any disturbances, which shift the normal balance of Na^+/ Ca^{2+} handling, will influence the NCX function. The altered function of NCX may lead to membrane potential instability and development of delayed afterdepolarizations (DADs).

Several diseases which increase the level of intracellular Na^+ by reduction of the activity of Na^+/K^+ pump function (hypoxic conditions or digitalis intoxication, **Figure 5**) or by increasing the I_{NaL} (long QT Syndrome 3 – LQT3) can lead to marked activation of reverse mode NCX function, which accounts for the concomitant Ca^{2+} accumulation and the subsequent abnormal automaticity (43). It is suggested that selective NCX inhibition by suppressing either the reverse or the forward mode may have antiarrhythmic effect during Na^+ induced Ca^{2+} load.

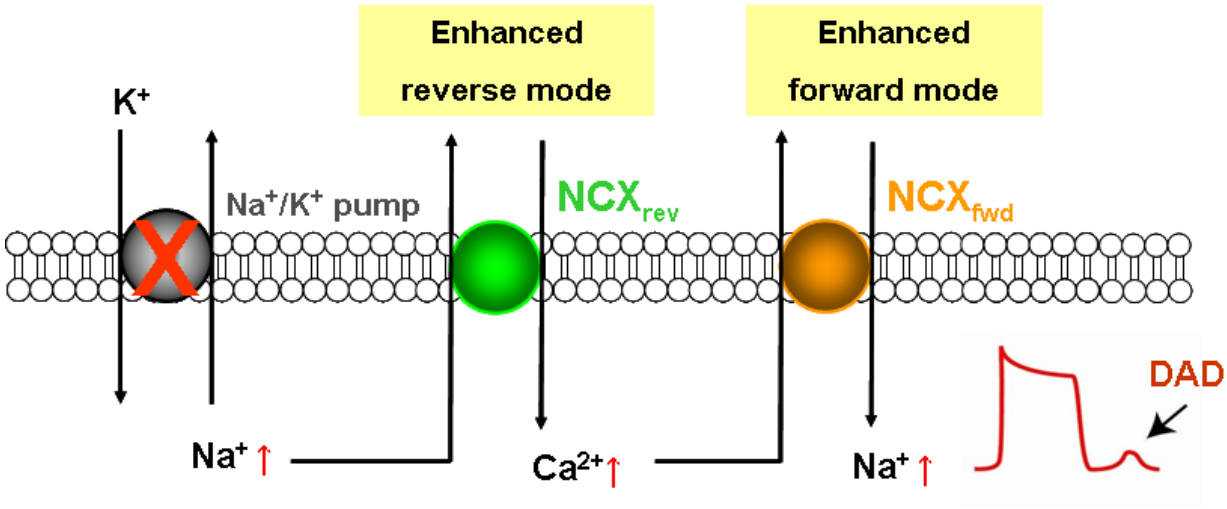

Figure 5. Schematic figure about the mechanism of elevated Na^+ induced triggered arrhythmias. *During Na^+/K^+ inhibition the Na^+ level is increased, which accumulates Ca^{2+} ions by stimulation of reverse mode NCX. This enhanced Ca^{2+} is able to evoke DAD formation, through increased forward NCX.*

The antiarrhythmic effect of selective NCX inhibition is controversial in the literature (43). NCX inhibitors have shown antiarrhythmic effects in hearth rhythm disturbances evoked by ischemia/reperfusion injury *in vivo* (44), in Langendorff perfused hearts (45-51), and in pharmacologically simulated ischemia/reperfusion models (52-56). The SEA0400 decreased the incidence (56), and reduced the development of EADs (57), it failed to suppress the aconitine induced arrhythmias (58). In Langendorff-perfused rat hearts SEA0400 even

enhanced the arrhythmia incidence and duration (59). The related studies from our laboratory are also contradictory. SEA0400 did not decrease QTc after dofetilide administration, and failed to prevent the development of Torsades de Pointes tachyarrhythmias (TdPs) in Langendorff-perfused rabbit hearts (30, 32), while in another study it effectively reduced the amplitudes of EADs, without influencing APD (56). In contrast, Milberg et al reported considerable APD shortening effect of SEA0400, furthermore, sotalol or veratridine induced TdPs were also suppressed (57, 60). Recently Jost et al. (10) claimed that ORM-10103, a novel NCX inhibitor with improved selectivity decreased pharmacologically induced DADs and EADs, confirming previous results performed with SEA0400 (56).

1.3. Summary of NCX inhibitors

Benzyloxyphenyl derivative inhibitors like KB-R7943, SEA0400, SN-6 were used successfully in several NCX studies (43). These compounds inhibit NCX from the external side. KB-R7943 was the first as a prototype in this NCX inhibitor family, which preferentially inhibits the reverse mode operation of NCX (61, 62). In cardiac cells the reverse mode blocking effect was larger compared with the forward mode (EC_{50}= 0.3 µM on reverse *vs*. 17 µM on forward mode). SEA0400 is a much more potent NCX blocker, EC_{50}=111 nM on the reverse *vs*. 108 nM on the forward mode, (63, 64), but both KB-R7943 and SEA0400 were shown to exert substantial nonspecific effects on several ion channels: I_{Na}, I_{CaL}, I_{K1} and delayed rectifier K^+ currents. SN-6 was developed from KB-R7943 (65), but it also more potently inhibits outward, than inward NCX current (EC_{50}= 1.9 µM *vs* 2.3 µM) and also significantly suppresses other currents (I_{Na}, I_{CaL}, I_{Kr}, I_{Ks}, I_{K1}), causing AP shortening. The exchanger inhibitory protein (XIP) was developed as NCX inhibitor protein, interacting with the Na^+ regulatory domain of the NCX and suppresses both transport modes (66). However, the XIP fails to penetrate through the sarcolemma, so it can be used only intracellularly in patch clamp experiments (67, 68).

Recently, novel promising NCX inhibitors, ORM-10103 and ORM-10962 have been developed. The ORM-10103 inhibited both modes of the NCX, and successfully suppressed *in vitro* the pharmacologically induced EADs and DADs (10) in dog heart preparations. With the exception of a 25.4% inhibition of the I_{Kr}, the ORM-10103 did not influence the major ionic currents. More recently, a novel compound, the ORM-10962 was synthesized exerting considerably lower EC_{50} levels with promising selectivity and antiarrhythmic profile (26).

1.4. Aims of the study

Since our knowledge about the role of NCX in the cardiac repolarization and in pacemaker activity is not fully clarified because of the lack of selective inhibitors, the aims of the present study were:

1) To analyse the effects of the newly synthesized NCX blockers ORM-10103 and ORM-10962 on the NCX current

2) To investigate the selectivity of ORM-10962 on major transmembrane ionic currents comparing with the results of ORM-10103

3) To study the effect of selective NCX inhibition on cardiac ventricular action potentials and on calcium transients

4) To investigate the role of NCX in the cardiac pacemaker function

5) To examine the effect of NCX inhibition on *in vitro* triggered arrhythmias

2. MATERIALS AND METHODS

2.1. Animals and ethical considerations

Adult mongrel dogs of either sex weighing 8 to 16 kg, New Zealand rabbits 2.5 to 3 kg and guinea-pigs 250-300 g obtained from a licensed supplier were used for the study. Following anticoagulation by sodium-heparin and xylazine (1 mg/kg, *i.v.*) or thiopental (30 mg/kg *i.v.*) induced anaesthesia, each heart was rapidly removed through a right lateral thoracotomy and immediately rinsed in oxygenated modified Locke's solution containing (in mM): NaCl 120, KCl 4, $CaCl_2$ 1, $MgCl_2$ 1, $NaHCO_3$ 22, and glucose 11. The pH of this solution was set between 7.35 and 7.4 when saturated with the mixture of 95% O_2 and 5% CO_2 at 37 ºC.

All experiments were conducted in compliance with the Guide for the Care and Use of Laboratory Animals (USA NIH publication No 85-23, revised 1996) and conformed to Directive 2010/63/EU of the European Parliament. The protocols were approved by the Review Board of the Department of Animal Health and Food Control of the Ministry of Agriculture and Rural Development, Hungary (XIII./1211/2012). The ARRIVE guidelines were adhered to during the study (NC3Rs Reporting Guidelines Working Group, 2010).

2.2. Cell preparations

2.2.1. Isolation of canine ventricular myocytes

Ventricular myocytes were enzymatically dissociated from canine hearts. For isolation of the single myocytes isolation solution was used with the following composition (mM) NaCl 135, KCl 4.7, KH_2PO_4 1.2, $MgSO_4$ 1.2, HEPES 10, $NaHCO_3$ 4.4, Glucose 10, $CaCl_2$ 1.8, (pH 7.2 with NaOH). A portion of the left ventricular wall containing an arterial branch was cannulated and perfused in a modified Langendorff apparatus at a pressure of 60 cmH_2O, with solutions in the following sequence: (*i*) isolation solution supplemented with $CaCl_2$ (1 mM) and sodium-heparin (0.5 ml) for 5-10 min to wash out the blood from the tissue; (*ii*) Ca^{2+} free isolation solution for 10 min; (*iii*) isolation solution (150 mL) supplemented with collagenase (type II, 250U/ml; Worthington) and 33 µM $CaCl_2$ for 15 min. Protease (type XIV, 0.04 mg·mL−1; Sigma Chemical) was added at the 15th minute of the third section of isolation and further 15-20 min of digestion was allowed. Portions of the left ventricular wall from the midmyocardial part were cut into small pieces in isolation solution supplemented with $CaCl_2$ (1 mM) for 15 min in 37°C. These tissue samples were then gently

agitated in a small beaker to dislodge single myocytes from the extracellular matrix. Throughout the entire isolation procedure, solutions were gassed with 100% O_2, while their temperature was maintained at 37°C. Myocytes were allowed to settle to the bottom of the beaker for 10 min, and then half of the supernatant was replaced with fresh solution. This procedure was repeated three times. Myocytes placed in isolation solution supplemented with $CaCl_2$ (1 mM) were maintained at 12–14°C before the experiment.

2.2.2. Isolation of rabbit sino-atrial node myocytes

For measuring I_f pacemaker current, we isolated single cells from the SAN region of rabbit heart by enzymatic dissociation. Untreated New-Zealand white rabbits (body weights 1.5-2 kg) of either sex were used for the study. The animals were sacrificed by cervical dislocation after receiving 400 IU/kg heparin intravenously. The chest was opened and the heart was quickly removed and placed into cold (4°C) solution with the following composition (mM): NaCl 135, KCl 4.7, KH_2PO_4 1.2, $MgSO_4$ 1.2, HEPES 10, $NaHCO_3$ 4.4, Glucose 10, $CaCl_2$ 1.8, (pH 7.2 with NaOH). The heart was mounted on a modified, 60 cm high Langendorff column and perfused with oxygenated and warmed (37°C) solution mentioned above. After washing out of blood (3-5 min) it was perfused with nominally Ca^{2+} free solution until the heart stopped beating (approx. 5 minutes). The digestion was performed by perfusion with the same solution supplemented with 1.8 mg/ml (260 U/ml) collagenase (Type II, Worthington). After 10-12 minutes the heart was removed from the cannula. Right atrium was cut and the crista terminalis and SAN region were excised and cut into small strips. Strips were placed into enzyme free solution containing 1mM $CaCl_2$ and equilibrated at 37°C for 10 minutes. After 10 minutes with gentle agitation, the cells were separated by filtering through nylon mesh. Sedimentation was used for harvesting cells. The supernatant was removed and replaced by HEPES buffered Tyrode's solution. The cells were stored at room temperature in the Tyrode's solution.

2.3. Voltage-clamp measurements

One drop of cell suspension was placed in a transparent recording chamber mounted on the stage of an inverted microscope (Olympus IX51, Tokyo, Japan), and individual myocytes were allowed to settle and adhere to the chamber bottom for at least 5-10 min before superfusion was initiated and maintained by gravity. Only rod-shaped cells with clear striations were used. HEPES-buffered Tyrode's solution (composition in mM: NaCl 144,

NaH_2PO_4 0.4, KCl 4.0, $CaCl_2$ 1.8, $MgSO_4$ 0.53, glucose 5.5 and HEPES 5.0, at pH of 7.4) was used as the normal superfusate.

Micropipettes were fabricated from borosilicate glass capillaries (Science Products GmbH, Hofheim, Germany), using a P-97 Flaming/Brown micropipette puller (Sutter Co, Novato, CA, USA), and had a resistance of 1.5-2.5 Mohm when filled with pipette solution. The membrane currents were recorded with Axopatch-200B amplifiers (Molecular Devices, Sunnyvale, CA, USA) by applying the whole-cell configuration of the patch-clamp technique. The membrane currents were digitized with 250 kHz analogue to digital converters (Digidata 1440A, Molecular Devices, Sunnyvale, CA, USA) under software control (pClamp 8 and pClamp 10, Molecular Devices, Sunnyvale, CA, USA).

2.3.1. Measurement of NCX current

For the measurement of the NCX current from single canine left ventricular myocytes the method of (69) was adapted and applied. Accordingly, the NCX current is defined as Ni^{2+}-sensitive current and measured in a special K^+-free solution (composition in mM: NaCl 135, CsCl 10, $CaCl_2$ 1, $MgCl_2$ 1, $BaCl_2$ 0.2, NaH_2PO_4 0.33, TEACl 10, HEPES 10, glucose 10 and ouabain 20 μM, nisoldipine 1 μM, and lidocaine 50 μM, at pH 7.4) after the formation of the whole cell configuration in HEPES-buffered Tyrode's solution at 37°C. The pipette solution used for recording NCX is contained: (in mM) CsOH 140, aspartic acid 75, TEACl 20, MgATP 5, HEPES 10, NaCl 20, EGTA 20 and $CaCl_2$ 10, pH was adjusted to 7.2 with CsOH. The $[Ca^{2+}]$ in the pipette was 160 nM by applying an appropriate mixture of $CaCl_2$ and EGTA as calculated by the WinMaxC software (70). After recording of control current, the test compounds ORM-10103 or ORM-10962 were applied and their effect were recorded, and finally 10 mM $NiCl_2$ was administrated to estimate the total NCX current. Therefore, the inhibited fraction was calculated as a subtracted current: the trace recorded in the presence of 10 mM $NiCl_2$ was subtracted from that measured in the absence of $NiCl_2$. The current-voltage (I-V) relationship of NCX was measured through the use of ramp pulses at 20 s intervals. The ramp pulse initially led to depolarization from the holding potential of -40 mV to 60 mV with a rate of 100 mV/s, then was hyperpolarized to -100 mV, and depolarized back to the holding potential. The descending limb of the ramp was utilized to plot the I-V curve.

2.3.2. Measurement of L-type calcium current

The L-type calcium current (I_{CaL}) was recorded from canine left ventricular myocytes in HEPES-buffered Tyrode's solution at 37°C supplemented with 3 mM 4-aminopyridine, to

block potassium currents. A special solution was used to fill the micropipettes (composition in mM: KOH 40, KCl 110, TEACl 20, MgATP 5, EGTA 10, HEPES 10 and GTP 0.25, pH was adjusted to 7.2 by KOH). I_{CaL} was evoked by 400 ms long depolarizing voltage pulses to various test potentials ranging from -35 mV to +40 mV. The holding potential was -80 mV. A short prepulse to -40 mV was used to inactivate fast inward Na^+ current. The amplitude of I_{CaL} was defined as the difference between the peak inward current at the beginning of the pulse and the current at the end of the pulse.

2.3.3. Measurement of potassium currents

The inward rectifier (I_{K1}), transient outward (I_{to}), rapid (I_{Kr}) and slow (I_{Ks}) delayed rectifier potassium currents were recorded in HEPES-buffered Tyrode's solution from isolated canine left ventricular myocytes at 37°C. The composition of the pipette solution (in mM) was the following: KOH 110, KCl 40, K_2ATP 5, $MgCl_2$ 5, EGTA 5, HEPES 10 and GTP 0.1 (pH was adjusted to 7.2 by aspartic acid). 1 µM nisoldipine was added to the bath solution to block I_{CaL}. When I_{Kr} was recorded I_{Ks} was inhibited by using the selective I_{Ks} blocker HMR 1556 (0.5 µM). During I_{Ks} measurements, I_{Kr} was blocked by 0.5 µM dofetilide and the bath solution contained 0.1 µM forskolin, to prevent the run-down of the current. The currents were activated by applying depolarizing voltage pulses.

Since the run-down of I_{CaL} and I_{Ks} currents is commonly seen during the measurements, the current level was monitored during the initial equilibration period and also at the end of the measurements when a washout period of at least 10 min was applied in order to draw a distinction between drug effect and run-down of the current. The cells, in which excessive run-down was observed, were omitted from the analysis.

2.3.4. Measurement of Na^+/K^+ pump current

Steady-state current at -30 mV was recorded in control conditions and in the presence of ORM-10962 from single canine left ventricular myocytes at 37°C. After 5-7 min incubation with ORM-10962 the normal external solution (composition in mM: NaCl 135, CsCl 2, KCl 5, $MgCl_2$ 1, $CdCl_2$ 0.2, $BaCl_2$ 2, HEPES 5, glucose 10, pH 7.4 by NaOH) was replaced by K^+ free solution. The Na^+/K^+ pump current (I_p) was defined as the difference between currents measured in 5 mM K^+ and in 0 mM K^+ containing solutions. The composition of the pipette solution (in mM) was: CsOH 100, aspartic acid 100, NaCl 30, MgATP 5, $MgCl_2$ 2, TEACl 20, EGTA 5, HEPES 10 and glucose 10 (pH was adjusted to 7.2 by CsOH).

2.3.5. Measurement of late sodium current

The late sodium current (I_{NaL}) is activated by depolarizing voltage pulses to -20 mV from the holding potential of -120 mV at 37°C in single left ventricular myocytes isolated from canine. After 5-7 min incubation with ORM-10962, 20 µM TTX was applied to achieve complete inhibition. The external solution was HEPES-buffered Tyrode's solution supplemented with 1 µM nisoldipine, 0.5 µM HMR-1556 and 0.1 µM dofetilide in order to block I_{CaL}, I_{Ks} and I_{Kr} currents. The composition of the pipette solution (in mM) was: KOH 110, KCl 40, K_2ATP 5, $MgCl_2$ 5, EGTA 5, HEPES 10 and GTP 0.1 (pH was adjusted to 7.2 by aspartic acid).

2.3.6. Measurement of the peak sodium current

The peak sodium current ($I_{Na\ peak}$) was measured in transfected CHO cell line (Chinese hamster ovary cells, ATCC, Manassas, Virginia, USA) with cDNA clone of the cardiac sodium channel Nav 1.5 (provided by Prof. Dr. György Panyi (71) from University of Debrecen, Medical and Health Science Center, Faculty of Medicine Department of Biophysics and Cell Biology). CHO cells were one day before the transfection cultured in 60 mm diameter culture dishes in F12 medium (Lonza, Verniers, Belgium) supplemented with 10% fetal bovine serum (PAA, Paschling, Austria) at 37 °C in CO_2 incubator (5% CO_2). Transient transfections were carried out by 20 µg polyethylenimine (25kDa, linear, Polysciences Inc., PA, USA) and 2µg of the Nav 1.5 plasmid DNA together with of 1µg GFP (green fluorescent protein) plasmid DNA combined in 1,5 ml serum-free F12 medium. The transfection mixture after 30 minutes incubation in room temperature was added to the washed cells with serum-free F12. After 2 hour incubation period in CO_2 incubator at 37 °C, the medium was changed for fresh growth medium. Transfected cells were trypsinized and centrifuged after 48 hours post transfection and re-suspended in growth medium. Cells were replaced in the bath and after 10 minutes superfused with HEPES-buffered Tyrode solution. The transfected cells were selected by GFP fluorescence in inverted fluorescent microscope (Olympus IX51). The $I_{Na\ peak}$ was recorded in GFP positive cells at room temperature (~23°C) with a following pipette solution (mM): KOH 110, KCl 40, K_2ATP 5, $MgCl_2$ 5, EGTA 5, HEPES 10 and GTP 0.1 (pH was adjusted to 7.2 by aspartic acid). Capacitance of the cells cancelled and series resistance was compensated to 70-80%. Current was elicited by step pulse into -20 mV from -90 mV holding potential for 20 ms.

2.3.7. Measurement of the pacemaker current

The I_f pacemaker current was recorded in HEPES-buffered Tyrode's solution at 37°C while the composition of the pipette solution was the following (in mM): KOH 110, KCl 40, K_2ATP 5, $MgCl_2$ 5, EGTA 5, HEPES 10 and GTP 0.1 (pH was adjusted to 7.2 by aspartic acid). For the measurement of the I_f current, the method of Verkerk et al (72) was adapted and applied. The current was activated by hyperpolarizing voltage pulses to -120 mV from the holding potential of -30 mV. The I_f was identified as ivabradine sensitive current (73).

2.4. Standard microelectrode technique

2.4.1. Action potential measurements in multicellular preparations

Adult mongrel dogs of either sex weighing 8-16 kg and New Zealand rabbits 2.5–3 kg were used. Dog papillary muscles preparations from the right ventricle were used for action potential measurements to investigate NCX role in shaping action potential and dog Purkinje fibres were prepared to investigate the effect of NCX inhibition on delayed afterdepolarizations triggered arrhythmias *in vitro*. Dog and rabbit free running Purkinje fibres and rabbit right atrial tissues were analysed for investigation of NCX role in pacemaker activity.

The preparations were placed in tissue chamber, superfused with oxygenated Locke's solution at 37 °C. Each preparation was stimulated (HSE stimulator type 215/II), initially at a constant cycle length of 1000 ms, with rectangular current pulses with 1 ms duration. The current pulses were isolated from ground and delivered through bipolar platinum electrodes in contact with the preparations. At least 1 h was allowed for each preparation to equilibrate during continuous superfusion with modified Locke's solution, warmed to 37 °C before the experimental measurements commenced. Transmembrane potentials were recorded with the use of conventional 5-20 MΩ, 3 M KCl-filled microelectrodes connected to the input of a high-impedance electrometer (Biologic Amplifier VF 102, Claix, France). In each experiment, the baseline action potential characteristics were first determined during continuous pacing at 1 Hz (on Purkinje fibres, continuous pacing at 2 Hz), and then when the pacing cycle length was sequentially varied from 300 to 5000 ms. The preparations were next superfused with the drug for 40-60 min before the pacing protocol was repeated and the parameters were measured again. Efforts were made to maintain the same impalement throughout each experiment. If impalement became dislodged, electrode adjustment was attempted and, if the action potential characteristics of the re-established impalement deviated by less than 5% from those of the previous measurement, the experiment was continued.

When this 5% limit was exceeded, the experiment was terminated and all the data involved were excluded from the analyses.

2.4.2. Recording of slow response action potentials

Adult guinea-pigs of either sex weighing 250-300 g were anticoagulated with sodium-heparin and anaesthetized with 30 mg/kg intravenous thiopental. The hearts were rapidly removed through a right lateral thoracotomy and immediately rinsed in ice-cold Krebs-Henseleit solution (containing in mM: NaCl 118.5, KCl 4.0, $CaCl_2$ 2.0, $MgSO_4$ 1.0, NaH_2PO_4 1.2, $NaHCO_3$ 25.0 and glucose 10.0). The pH of this solution was set to 7.35±0.05 when saturated with a mixture of 95% O_2 and 5% CO_2. After excision, the right or left ventricular papillary muscle preparations were immediately mounted in a 40 ml tissue chamber, and initially perfused with normal Krebs-Henseleit solution.

The preparations were stimulated (Experimetria Ltd, PW-01, Hungary) by constant rectangular voltage pulses (1 ms) delivered through a pair of bipolar platinum electrodes at a frequency of 1 Hz. Action potentials were recorded with a conventional microelectrode technique. Sharp microelectrodes, with a tip resistance of 10-20 MΩ when filled with 3 M KCl, were connected to the amplifier (Biologic Amplifier VF 102, Claix, France). The voltage output from the amplifier was sampled with an AD converter (NI 6025, Unisip Ltd, Hungary). The action potential amplitude and maximum rate of depolarization were obtained with Evokewave v1.49 software (Unisip Ltd, Hungary). Each preparation was allowed for at least 30 min to equilibrate in normal Krebs-Henseleit solution at 37 °C. Slow response action potentials were established in modified Locke's solution containing 25 mM KCl, supplemented with 100 µM $BaCl_2$ to inhibit I_{K1} and with 1 µM forskolin to facilitate I_{CaL}. The dV/dtmax values in the interval of 5-20 V/s, and amplitudes of at least 60 mV were accepted; data from experiments deviating from these ranges were discarded.

2.5. Ca^{2+} transient and cell shortening measurements

Myocytes were loaded with Fluo-4 AM (5 µM) for 15 min at room temperature in Tyrode's solution. One drop of the cells was placed in a cell chamber (RC47FSLP, Warner Instruments, Hamden, CT, USA) and were field stimulated at 1 Hz with a stimulator (PW-01, Experimetria Ltd. Hungary). The measurement was performed on an inverted microscope (Olympus IX 71; Olympus, Tokyo, Japan). The fluorescent dye was excited at 480 nm and emitted at 535 nm. Ca^{2+} signals were recorded by a photon counting photomultiplier module

(Hamamatsu, model H7828; Hamamatsu Photonics Deutschland GmbH, Herrsching am Ammersee, Germany) and were digitized and sampled at 1 kHz by using Digidata 1440A interface (Axon Instruments). The data acquisition and analysis were performed by pClamp 10.0 (Molecular Devices, USA). The transient amplitudes were calculated as a difference of the peak and diastolic fluorescent values. Background fluorescence levels were used to correct raw fluorescence data. The Ca^{2+} transients were normalized to the diastolic fluorescent level. The cell shortening was measured by using a video edge detector system (VED-105, Crescent Electronics, Sandy, Utah, USA).

The control transients in physiological NCX conditions were monitored in a normal HEPES-buffered Tyrode's solution (containing in mM: 144 NaCl, 0.4 NaH_2PO_4, 4 KCl, 0.53 $MgSO_4$, 1.8 $CaCl_2$, 5.5 glucose and 5 HEPES; pH was adjusted to 7.4 with NaOH). To analyze the CaTs in enhanced NCX reverse mode the solution was switched to modified Tyrode's solution containing 70 mM NaCl and 70 mM cholin-cloride. The CaTs in enhanced NCX forward mode was investigated in normal Tyrode's solution supplemented with 600 nM forskolin. After recording the control transients in the three groups, 1 µM ORM-10962 were added to the solution.

2.6. Chemicals

With the exception of ORM-10103 and ORM-10962 (Orion Pharma, Espoo, Finland), HMR-1556 (Tocris Bioscience, Tocris House, Bristol, UK) and nisoldipine (gift from Bayer AG, Leverkusen, Germany) all chemicals were purchased from Sigma-Aldrich Fine Chemicals (St. Louis, MO, USA). ORM-10103 and ORM-10962 were dissolved in DMSO to yield a 1 mM stock solution. This stock solution was diluted to reach the desired final concentration (DMSO concentration not exceeding 0.1 %) in the bath.

2.7. Statistics

All data are expressed as means ± SEM. Statistical analysis was performed with Student's t-test for paired data. The results were considered statistically significant when p was < 0.05.

3. RESULTS

3.1. Chemical structures of ORM-10103 and ORM-10962

ORM-10103 [5-nitro-2-(2-phenylchroman-6-yloxy) pyridine] and ORM-10962 [2-(4-hydroxypiperidin-1-yl)-N-(6-((2-phenylchroman-6-yl)oxy)yridine-3-yl)acetamide] was put at disposal by Orion Pharma (Espoo, Finland) and its structure is depicted in **Figure 6.**

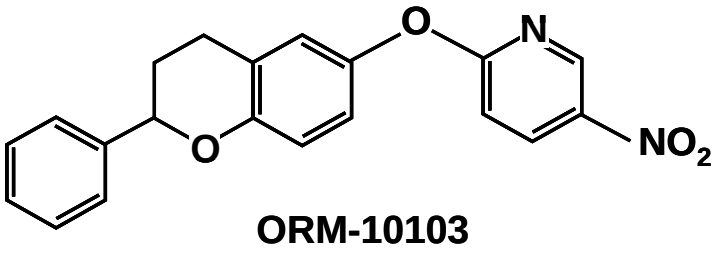

ORM-10103

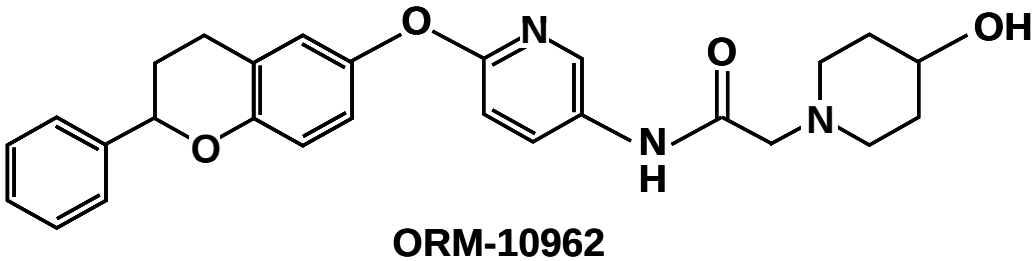

ORM-10962

Figure 6. The chemical structures of ORM-10103 and ORM-10962.

3.2. Inhibition of NCX current by ORM-10103 and ORM-10962

NCX current was determined during the voltage ramp pulse, after blocking other currents (Na^+, Ca^{2+}, K^+ and Na^+/K^+ pump) in isolated canine left ventricular cardiomyocytes. After the control records ORM compounds were applied and the current was recorded with the same voltage pulse. Finally, 10 mM $NiCl_2$ was added to the bath solution for the complete inhibition of the NCX current and this trace was subtracted from the control record and from the ORMs records resulting in Ni^{2+} sensitive current traces in control conditions and in the presence of ORMs.

As shown in **Figure 7,** ORM-10103 applied at 10 µM concentration caused a comparable, significant inhibition of NCX both in the reverse as well as in the forward mode operation (82±9% and 88±6% inhibition, respectively, n=6 cell/2 hearts). The estimated EC_{50} values for the inward and outward NCX currents were 780 nM, and 960 nM (10), however, a

small but statistically significant inhibition on the I_{Kr} indicated the importance of development of novel NCX inhibitor compounds with better selectivity profile and lower EC_{50} values. Therefore, we aimed to analyse the recently synthesized NCX inhibitor compound ORM-10962.

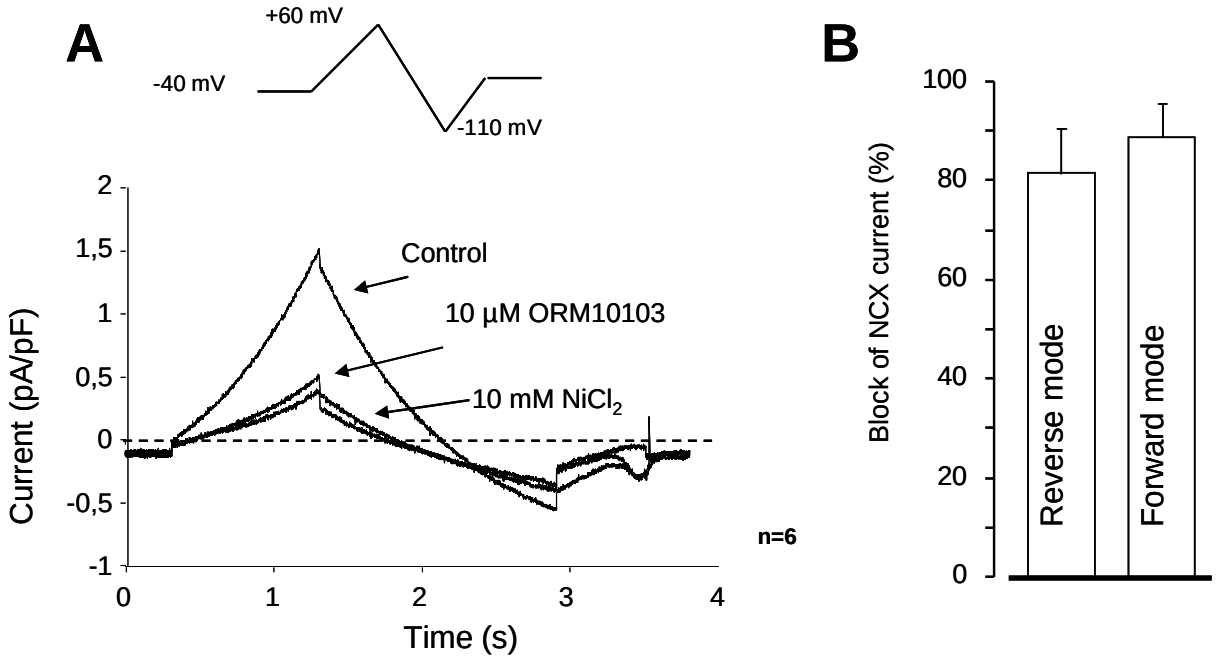

Figure 7. Effect of NCX inhibition by ORM-10103. Panel A. *NCX was determined using the conventional ramp protocol and defined as a Ni^{2+}-sensitive current. Original measurement shows the NCX curve before and after applying 10 µM ORM-10103. 10mM $NiCl_2$ was used for complete inhibition.* **Panel B.** *Bar graphs represent 10 µM ORM-10103 efficiently inhibited NCX in both transport modes of the exchanger. The inhibition in the reverse mode was 82±9 % measured at +40 mV in forward was 88±6 %, measures at -80 mV. Values are means ± standard errors of the means (n=6).*

As **Figure 8** illustrates, ORM-10962 considerably decreased both the outward and the inward NCX current in a concentration-dependent manner. The effect of the drug at different concentrations on the outward NCX current (reverse mode) was calculated at 20 mV and on the inward current (forward mode) was determined at -80 mV. Concentration-response relations for both reverse and forward modes were fitted by Hill function. The estimated EC_{50} values of ORM-10962 for the outward and inward NCX currents were found to be 67 nM, and 55 nM, respectively (**Figure 8.**).

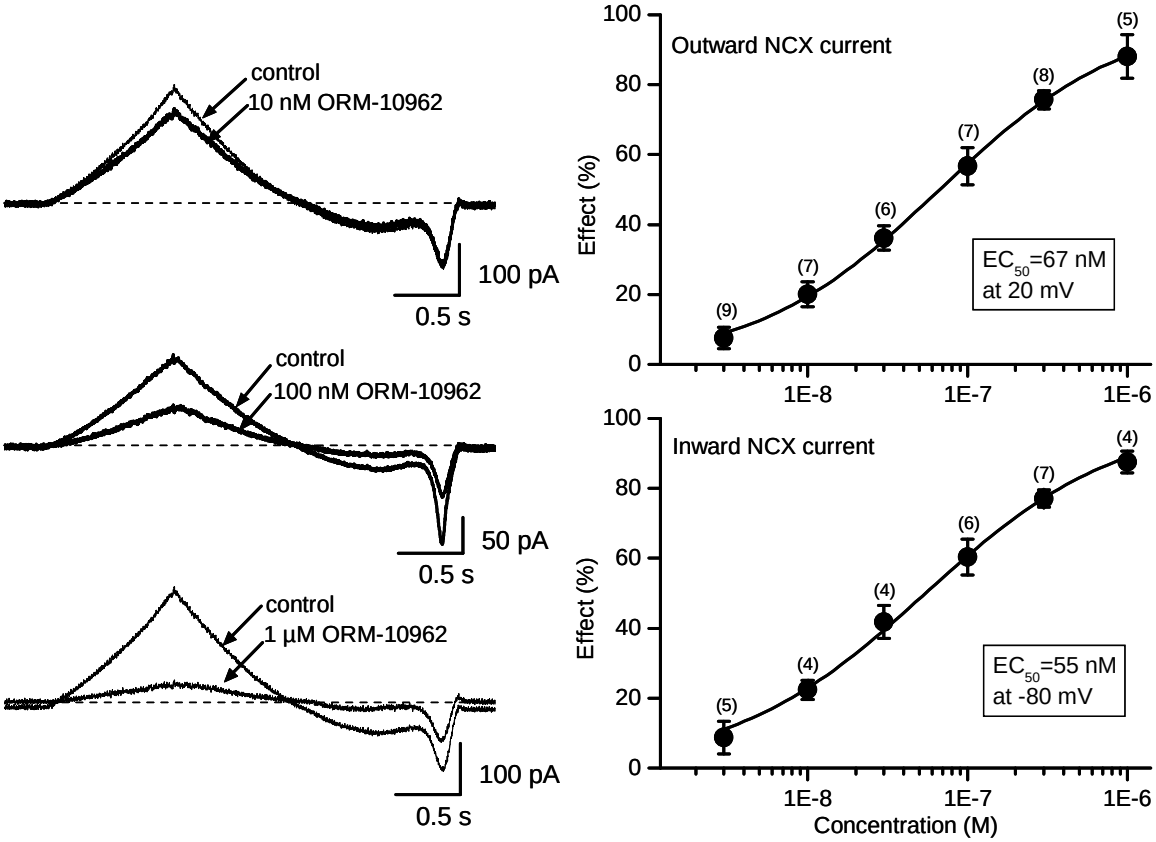

Figure 8. Effect of NCX inhibition by ORM-10962. Left panel shows the concentration-dependent effect of ORM-10962 on the NCX current. *Each panel presents Ni^{2+}-sensitive NCX current traces before and after superfusion of the cells with ORM-10962 at concentrations of 10 nM, 100 nM and 1 µM. In the right panel the drug-response curves presented of ORM-10962 on the outward (top) and inward (bottom) NCX currents in canine ventricular myocytes are given at 20 mV and at -80 mV, respectively. Values are means ± SEM, n=4-9.*

3.3. Selectivity of ORM-10962

3.3.1. The effect of ORM-10962 on the L-type inward calcium current

The possible effect of ORM-10962 on the I_{CaL} was investigated in single dog ventricular myocytes. The following protocol was used for patch clamp measurements: the holding potential was -80 mV and a short prepulse to -40 mV was added to inactivate I_{Na}. I_{CaL} was activated by 400 ms long depolarizing voltage pulses to different test potentials ranging from -35 mV to 55 mV. These experiments clearly revealed that ORM-10962 even at high (1 µM) concentration did not influence I_{CaL} (**Figure 9.A**). Indeed, after the application of ORM-10962, a small but significant decrease of the current was observed, which was maintained during the wash out. This slight further decrease showed that the marginal reduction of the current amplitude in the presence of ORM-10962 was a consequence of the run-down phenomenon of the I_{CaL}.

The effect of ORM-10962 was also studied on slow response action potentials recorded from guinea-pig papillary muscles. As **Figure 9. B** shows, ORM-10962 at 1 µM did not affect the amplitude (control: 73.2±0.7 mV, ORM-10962: 72.1±4.9 mV, n = 5, n.s.) or dV/dtmax (control: 17.6±0.7 V/s, ORM-10962: 16.6±0.9 V/s, n = 5, n.s.) of the slow response action potentials, which may support the results of the direct I_{CaL} measurements. In the same preparations for positive control we used a well-established I_{CaL} blocker nisoldipine at 100 nM, which markedly reduced both the amplitude and dV/dtmax of the slow response action potentials (73.2±0.7 mV *vs* 44. 2±1.5 mV and 17.6±0.7 V/s *vs* 5.9±1.5 V/s, respectively; n=5, p<0.05).

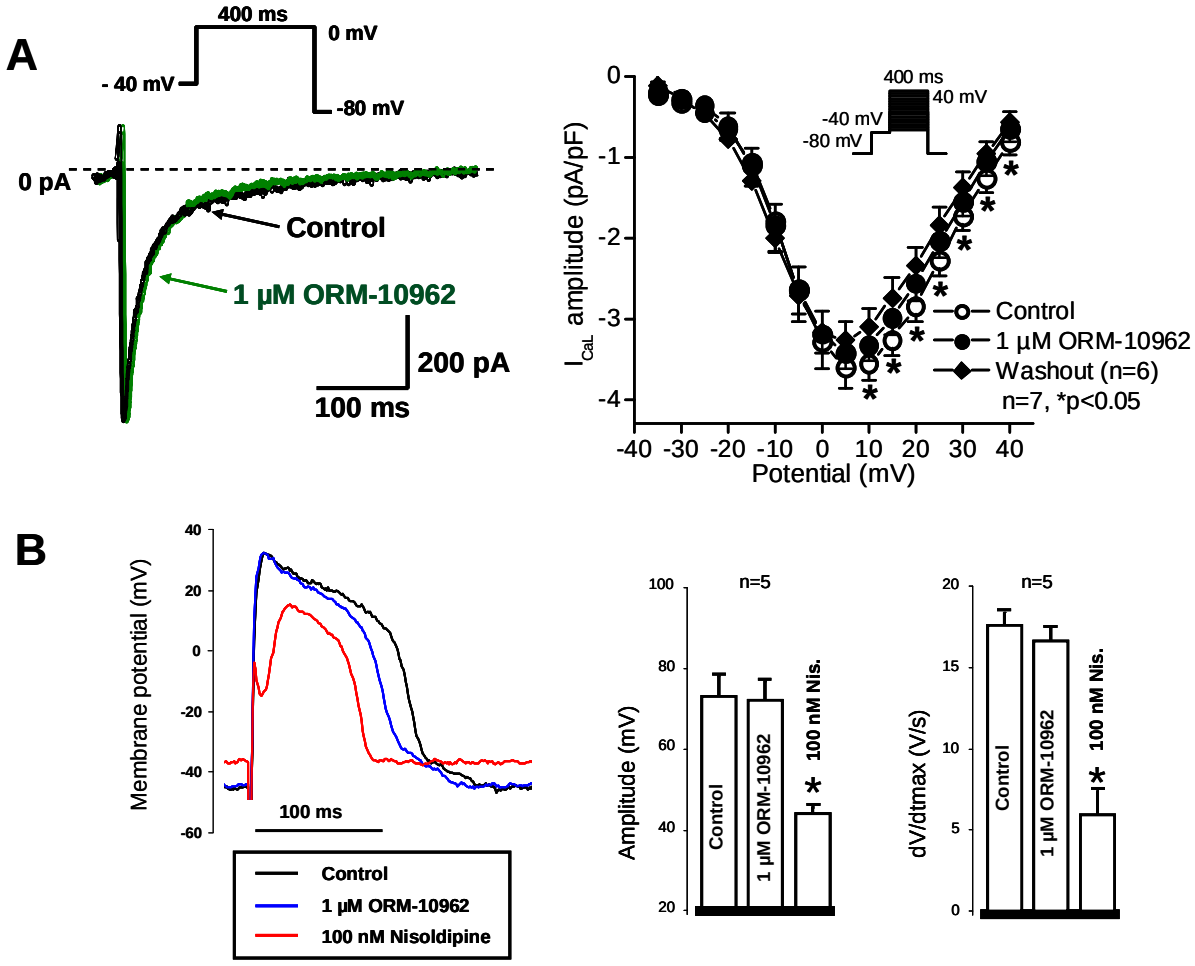

Figure 9. Lack of effect of 1µM ORM-10962 on the I_{CaL}. Panel A. *The left panel illustrates original I_{CaL} traces before and after application of 1 µM ORM-10962 in dog ventricular myocytes. The right panel shows the current-voltage relation of I_{CaL} in the absence and presence of 1 µM ORM-10962, as well as after wash out of ORM-10962. Values are means ± standard errors of the means, n= 7, p<0.05. Inset shows the applied voltage protocol.* **Panel B.** *shows the lack of effect of 1µM ORM-10962 on slow response action potentials in guinea-pig ventricular myocytes at 1Hz: original slow AP recordings under control conditions, in the presence of 1 µM ORM-10962, and after application of 100 nM nisoldipine. Bar diagrams reveal the lack of effect of 1 µM ORM-10962 on the action potential amplitude and on the maximum rate of depolarization, respectively (n=5, p<0.05).*

3.3.2. The effect of ORM-10962 on late and peak sodium current, and on Na^+/K^+ pump currents

The possible effect of ORM-10962 on the late sodium current (I_{NaL}) was also studied in dog left ventricular myocytes. The current was activated by depolarizing pulses to -20 mV from a holding potential of -120 mV. Addition of 1 µM ORM-10962 did not decrease the amplitude of I_{NaL} while 20 µM TTX completely blocked the current (**Figure 10.A**). The amplitude of the TTX sensitive I_{NaL} was -0.63±0.13 pA/pF in control conditions and -0.65±0.14 pA/pF after application of 1 µM ORM-10962 (n = 5, n.s.).

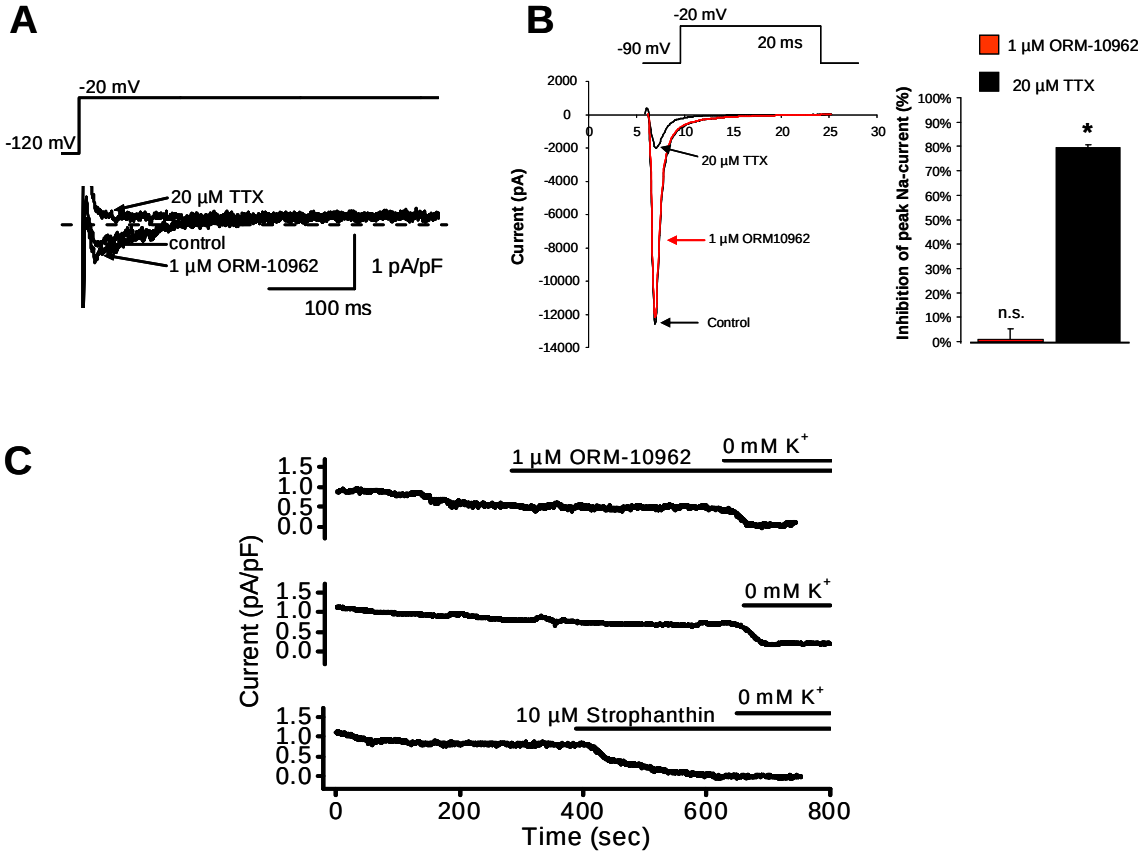

Figure 10. Lack of effect of ORM-10962 on I_{NaL}, $I_{Na\ peak}$, and Na^+/K^+ pump current. *The onset on the top of the figure shows the applied voltage protocol and the original current traces.* **Panel A.** *shows that 1 µM ORM-10962 does not influence I_{NaL}, while 20 µM TTX blocks the current.* **Panel B.** *I_{Na} peak was not significantly changed after the application of 1 µM ORM-10962, however 20 µM TTX markedly decreased the amplitude of the current. Bar graphs represent the inhibition of $I_{Na\ peak}$ by 1 µM ORM-10962 compared to 20 µM TTX, ($n=5$, $p<0.05$).* **Panel C.** *Lack of effect of ORM-10962 on Na^+/K^+ pump current. I_p was specified as a steady-state difference current between currents measured in 5 mM K^+ and in 0 mM K^+ containing solutions. The current traces were recorded at a steady potential of -30 mV. Top trace shows that application of 1 µM ORM-10962 does not influence I_p, however, a slight gradual decrease of the current was observed. An original current record in middle trace as a time control, indicates a slight gradual current decrease (similar to that shown in top trace), which was also observed without addition of ORM-10962. Bottom trace is the positive control. Application of 10 µM strophantin completely blocks Na^+/K^+ pump current.*

The peak sodium current ($I_{Na,peak}$) was measured in Nav1.5 overexpressed CHO cells at -20 mV depolarizing pulses from a holding potential of -90 mV (**Figure 10.B**). After applying 1 µM ORM-10962 the control $I_{Na,peak}$ was not significantly changed (-806.6±299 pA/pF vs -782.7±257 pA/pF after 1 µM ORM-10962; Δ=1.06±0.04 %) however, after 20 µM TTX the current markedly reduced (152.8±47.9 pA/pF; Δ=79.6±0.01 %; n=10, $p<0.05$).

The Na^+/K^+ pump current (I_p) was measured as a steady-state current at -30 mV. In control conditions I_p was 0.46±0.10 pA/pF and it decreased to 0.39±0.11 pA/pF (Δ=16.2%, n=5, $p<0.05$) at the end of the 5–7 min incubation with 1 µM ORM-10962. During the measurements a gradual slight decrease of the steady-state current was observed (**Figure 10. C** top trace). Therefore, a time control was made in a separate set of experiments when the same protocol was applied with the vehicle of the ORM-10962 (DMSO). Similar small current decrease was recorded (0.55±0.10 pA/pF vs. 0.44±0.06 pA/pF, Δ=21.5 %, n=3, **Figure 10. C** middle trace) in the steady-state current which was observed in the presence of the ORM-10962. Therefore, it is concluded that ORM-10962 does not influence Ip, the slight tendency of the current to decrease is not due to the effect of ORM-10962. For positive control 10 µM strophantin was used, which is a well-known blocker of Na^+/K^+ pump. Strophantin effectively suppressed the current and subsequent addition of 0 mM K^+ solution failed to cause further decrease in the Na^+/K^+ pump current justifying the complete inhibition of the current after strophantin application (**Figure 10. C** bottom trace).

3.3.3. The effect of ORM-10962 on outward potassium currents

The effect of ORM-10962 on I_{K1}, I_{to}, I_{Kr} and I_{Ks} were also investigated. The I_{K1} was measured by determining the steady-state current-voltage relationship of the membrane at the end of 300 ms long pulses clamped to potentials ranging from -80 to 0 mV. I_{to} was activated by 1000 ms long depolarizing voltage pulses arising from the holding potential of -80 mV to test potentials gradually increasing up to 50 mV. I_{Kr} and I_{Ks} were determined as tail current amplitudes at -40 mV after activating these currents by 1000 ms (I_{Kr}) or 5000 ms (I_{Ks}) long depolarizing voltage pulses at various test potentials ranging up to 50 mV. It was found that neither of these currents was significantly influenced by 1 µM ORM-10962 (**Figure 11.**).

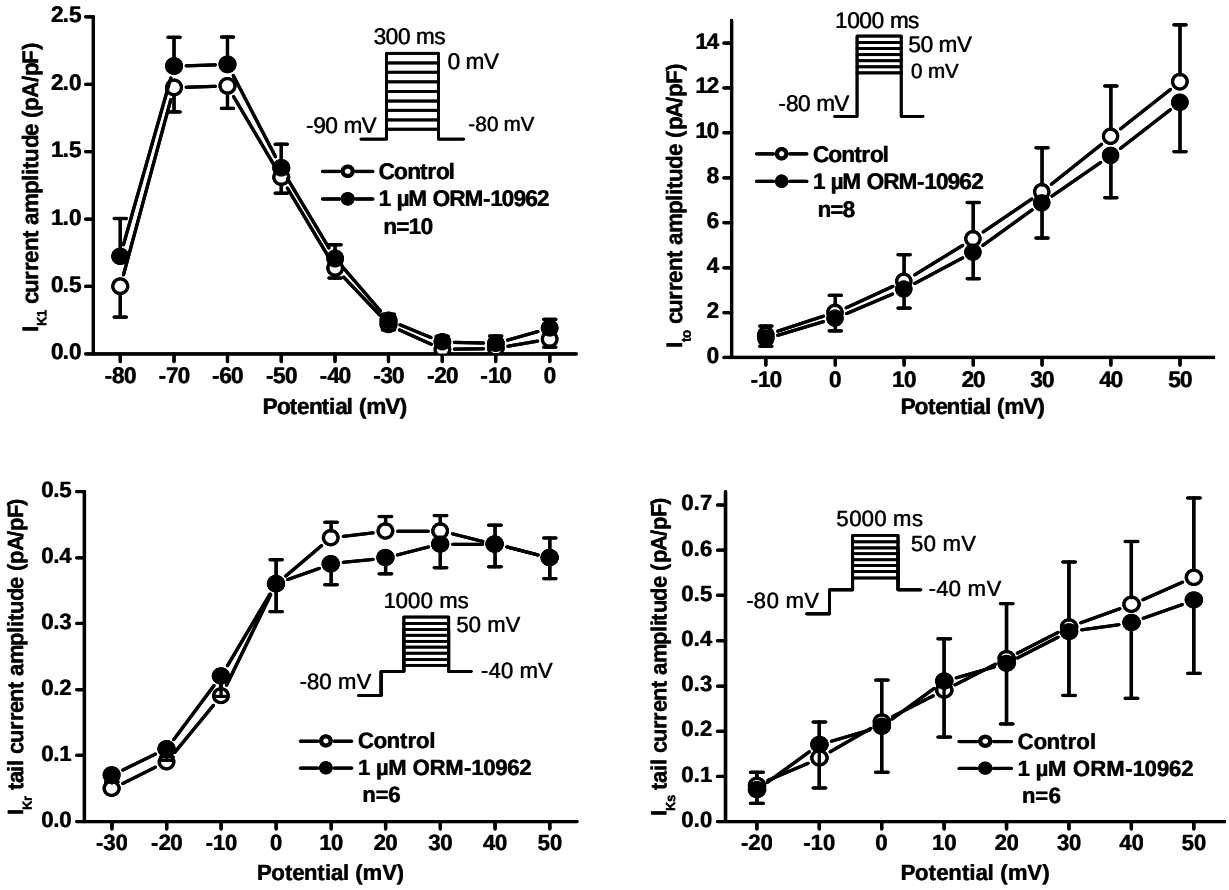

Figure 11. Lack of the effect of ORM-10962 on main repolarizing potassium currents. *Current-voltage curves of I_{K1}, I_{to}, I_{Kr} and I_{Ks} represent the currents before and after of applying 1 μM ORM-10963. Insets show the applied voltage protocols. Values are means ±SEM.*

3.3.4. Selectivity of ORM-10962 on the pacemaker current

The effect of ORM-10962 on the I_f was investigated in rabbit right atrial cells isolated from the SAN region. For the measurement of the I_f, the method of Verkerk and co-workers (72) was adapted and applied. The current was activated by hyperpolarizing voltage pulses to -120 mV from the holding potential of -30 mV. The pacemaker current was identified as ivabradine sensitive current (73). As **Figure 12.** shows, at negative hyperpolarizing membrane potential (from -30 mV to -120 mV) an ivabradine (10 μM) sensitive current could be measured, which was not altered after application of 1 μM ORM-10962.

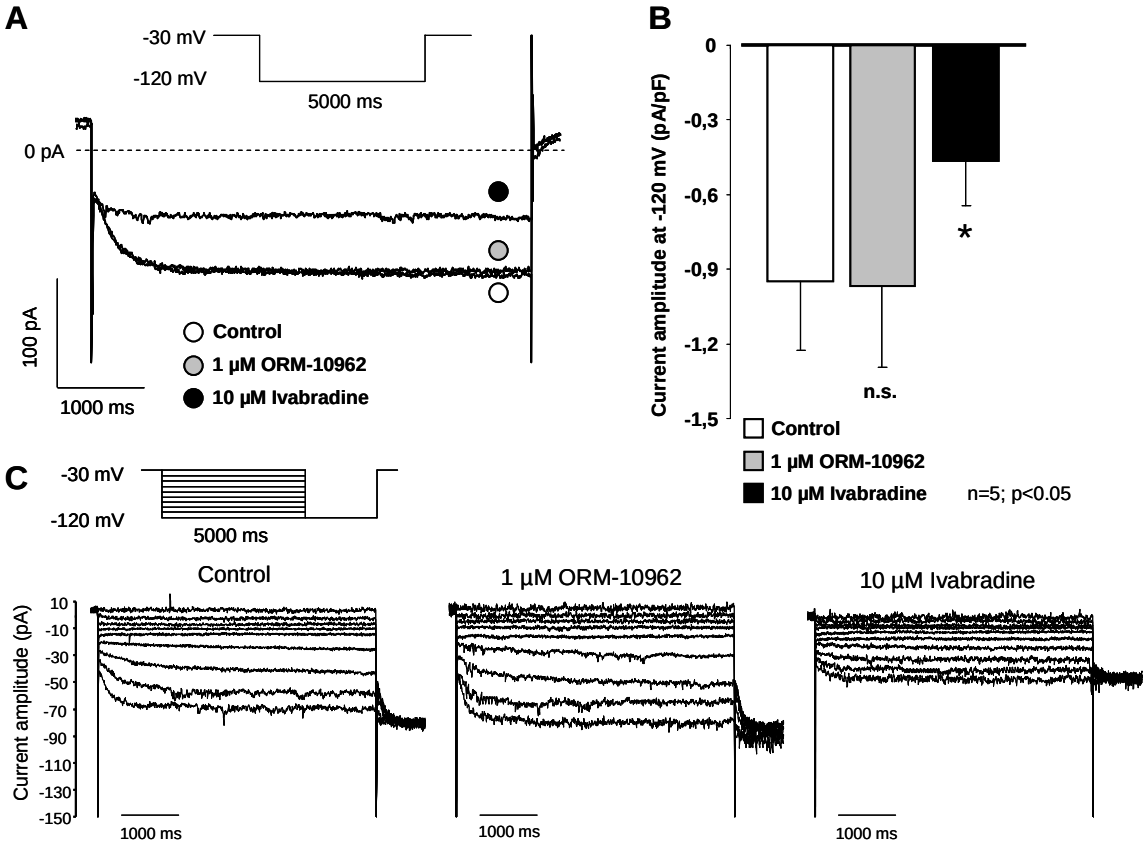

Figure 12. Lack of effect of 1µM ORM-10962 on the pacemaker current in rabbit SAN myocytes. Panel A. *Original recording of I_f current is depicted under control condition, in the presence of 1 µM ORM-10962 and after application of 10 µM ivabradine, as a positive control. The inset shows the applied voltage protocol. In* **Panel B.** *bars represents the current amplitude measured at -120 mV hyperpolarizing pulses, by comparing the current maximum at the beginning of the pulse, with the mean current in the steady-state section of the current. 1 µM ORM-10962 did not alter significantly the current, while 10 µM ivabradine exerted marked effect. Values are means ± SEM.* **Panel C.** *shows representative voltage-current pulses in control, after application of 1 µM ORM-10962 and subsequently applied 10 µM ivabradine, as a positive control. I_f was elicited by rectangular hyperpolarizing voltage steps from a holding potential of -30 mV to -120 mV for 5000 ms.*

3.4. Comparison of the effects of ORM-10103 and ORM-10962 on the major repolarizing transmembrane potassium currents

The I_{K1} did not show significant change after application either of 10 µM ORM-10103 or 1µM ORM-10926 (control: 2.03±0.25 pA/pF *vs* 10µM ORM-10103: 2.38±0.31 pA/pF, n=11, n.s.; control: 1.99±0.16 pA/pF *vs* 1µM ORM-10962: 2.14±0.21 pA/pF, n=10, n.s) as illustrated at -60 mV (**Figure 13.A).**

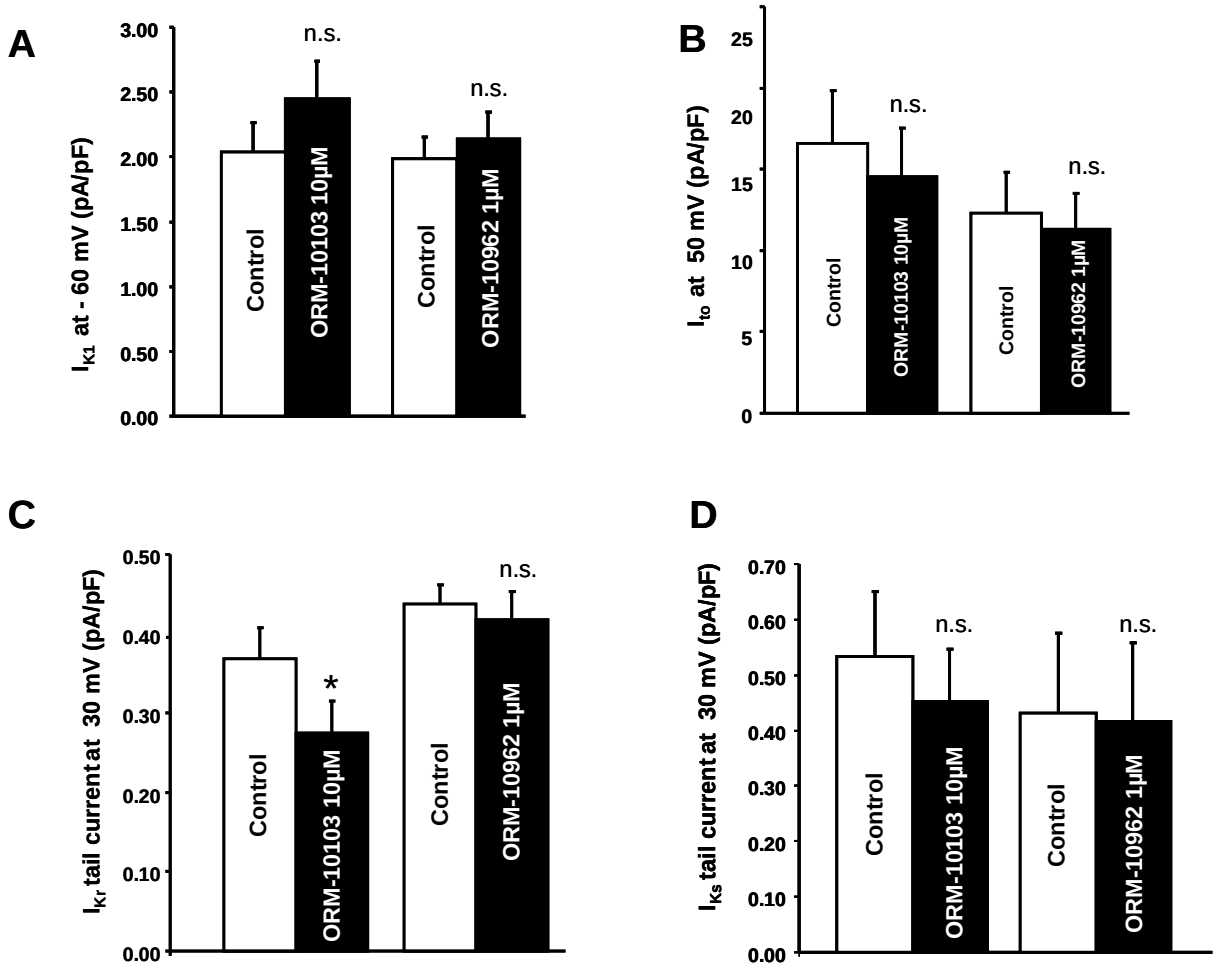

Figure 13. Comparison of the effect of ORM-10103 and ORM-10962 on the major repolarizing transmembrane potassium currents. Panel A, **B**, **C**, *and* **D** *represent the I_{K1}, I_{to}, I_{Kr}, and I_{Ks} respectively. The only difference was found in I_{Kr} where 10µM ORM-10103 significantly decreased the current magnitude while 1 µM ORM-10962 did not change the tail current. Values are means ± SEM, n= 6-11, p<0.05.*

Similarly, the I_{to} also was not changed by exposure to ORM-compounds (**Figure 13.B**) (control: 16.60±3.26 pA/pF *vs* 10 µM ORM-10103: 14.53±2.98 pA/pF n=9, n.s; control: 12.26±2.54 pA/pF *vs* 1 µM ORM-10926: 11.34±2.17 pA/pF, n=8, n.s.).

The I_{Kr} tail was analyzed at 30mV pulse (**Figure 13.C**). In contrast, 10 µM ORM-10103 significantly decreased the I_{Kr} amplitude (control: 0.37±0.04 pA/pF *vs* 10 µM ORM-10103: 0.28±0.04 pA/pF, Δ=25.4 %, n=8, p<0.05), however 1 µM ORM-10962 did not change the current (control: 0.44±0.02 pA/pF *vs* 0.42±0.04 pA/pF after 1µM ORM-10962 n=6, n.s.). The I_{Ks} tail was also identical after administration of ORM-compounds compared with the control measurements. (**Figure 13.D**, control: 0.53±0.12 pA/pF *vs* 10µM ORM-10103: 0.45±0.10 pA/pF, n=10, n.s.; control: 0.43±0.14 pA/pF *vs* 1µM ORM-10926: 0.42±0.14 pA/pF, n=6, n.s.).

3.5. Effect of selective NCX inhibition on Ca^{2+} transient and action potentials under normal condition

The calcium transients (CaT) and cell shortening were measured in normal Tyrode's solution. After registration of the control, the perfusion was switched to 1 µM ORM-10962 containing normal Tyrode's solution (**Figures 14. A** and **C**).

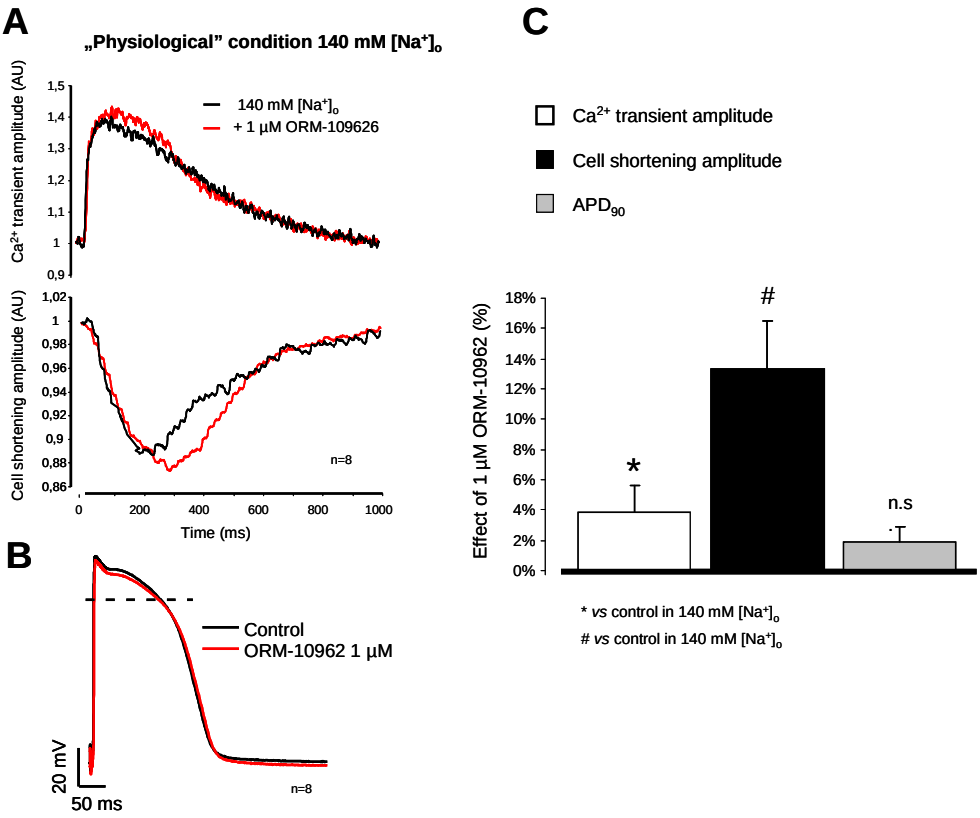

Figure 14. Effect of ORM-10962 on calcium transient, cell shortening, and action potential. Panel A. *CaTs and cell shortenings were simultaneously measured in isolated dog ventricular myocytes under normal conditions. The cells were loaded with Fluo-4AM fluorescent dye, and were field stimulated at 1 Hz. A small, but statistically significant increase in the transient and cell shortening magnitude were measured after application of 1 µM ORM-10962 (red line).* ***Panel B.*** *The APs were measured by using the conventional microelectrode technique in dog right papillary muscles. 1 µM ORM-10962 failed to influence the action potential characteristic.* ***Panel C.*** *The effects of ORM-10962 on CaT amplitude (white column), cell shortening (black column) and on APD_{90} (gray column) were compared in bar graph. Values are means ± SEM.*

The amplitude of Ca^{2+} transients and cell shortening slightly but statistically significantly increased after the addition of 1 µM ORM-10962: 15.03±2.16 AU *vs* 15.48±2.10* AU Δ=3.80±1.49%*, n=8, $p<0.05$; Cell shortening: -2.03±0.92 AU *vs* -2.35±1.05* AU, Δ=15.59±3.01%*, n=8, $p<0.05$. The diastolic Ca^{2+} did not change significantly (data not shown) during the experiment. The characteristic of the AP did not

change after application of 1 µM ORM-10962 (APD_{90}: 218.4±10.85 ms *vs* 222.5±9.66 ms; Δ=1.86±1.55 %; n=8, n.s.; **Figure 14. B** and **C**).

3.6. Effect of selective NCX inhibition on endocardial, epicardial tissues and on Purkinje fibres

We also studied the effect of ORM-10962 on AP in different canine ventricular tissue preparations, to investigate the role of NCX in transmural heterogeneity. In subendocardial multicellular preparation (**Figure 15.**) we observed a moderate increase in the APD parameters after application of 1µM ORM-10962 (APD_{90}=218.4±10.8 ms *vs* 222.5±9.6 ms APD_{75}= 203.5±10.6 ms *vs* 208.6±9.2 ms*; APD_{50}=175.6±10 ms *vs* 181.6±8.5 ms*; n=8, p<0.05). In subepicardial preparation the APD increased (APD_{90}= 212±5.4 ms *vs* 217.7±5.2 ms*; APD_{75}=199.5±5 ms *vs* 206.4±5.2 ms*; APD_{50}= 174.6±5.5 ms *vs* 184.4±6 ms*; n=7, p<0.05).

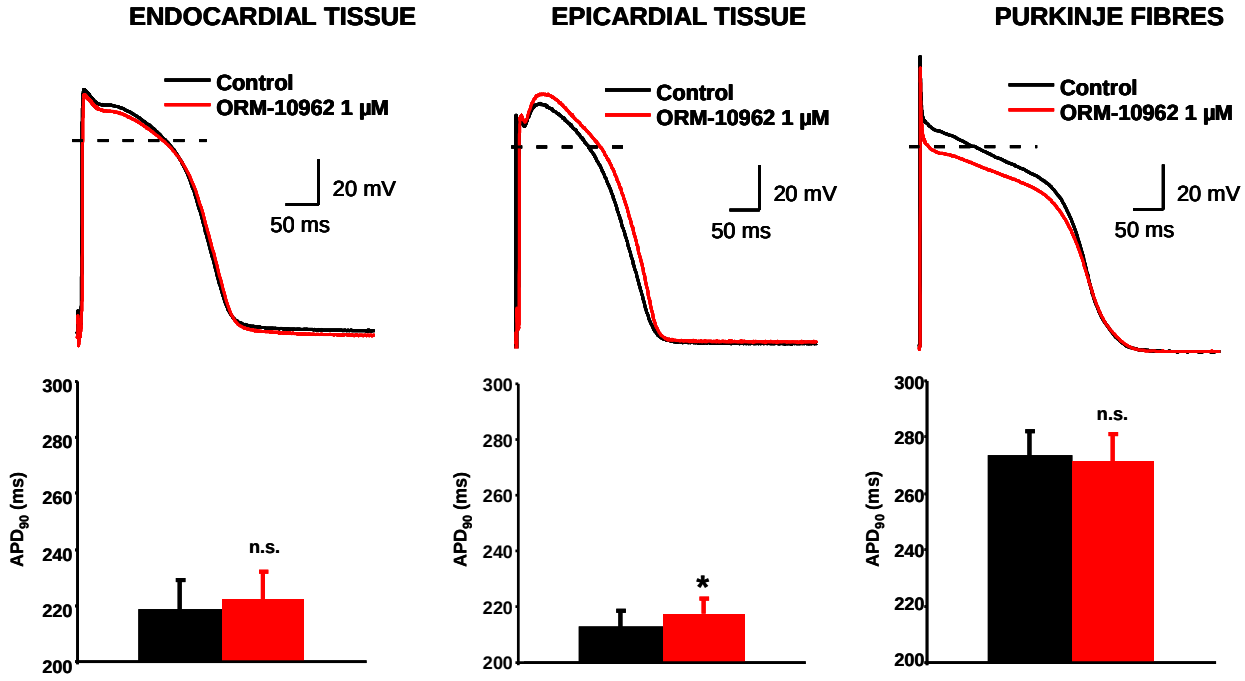

Figure 15. Effect of ORM-10962 on the action potential waveforms from different regional tissue preparations. *Original recordings obtained from papillary muscle (subendocardial) preparation (left), epicardial multicellular preparations (middle) and from Purkinje fibres (right). The bars represent the APD_{90} before and after application of 1 µM ORM-10962, p<0.05, n=7-8. Values are means ± SEM.*

The Purkinje fibre preparations exerted inconsistent and negligible change in the action potential duration (n=8), where a negative shift of the plateau voltage was observed without any significant changes in the repolarization parameters. Although in certain

preparations the relatively minor changes in the AP waveforms did not reach statistically significant differences in the averaged parameters, looking carefully the individual experiments, minor and variable repolarization changes could be often noticed. This suggests that a small NCX current may have some slight influence on cardiac repolarization depending on voltage and the actual intracellular Na^+ and Ca^{2+} level. In accordance with this observation baseline AP and intracellular Ca^{2+} waveforms vary experiment by experiment suggesting that the transmembrane current generated by NCX may reflect this variability.

3.7. Effect of NCX inhibition on the spontaneous automaticity

3.7.1. Effect of NCX inhibition on spontaneous automaticity on Purkinje fibres and on atrial tissue

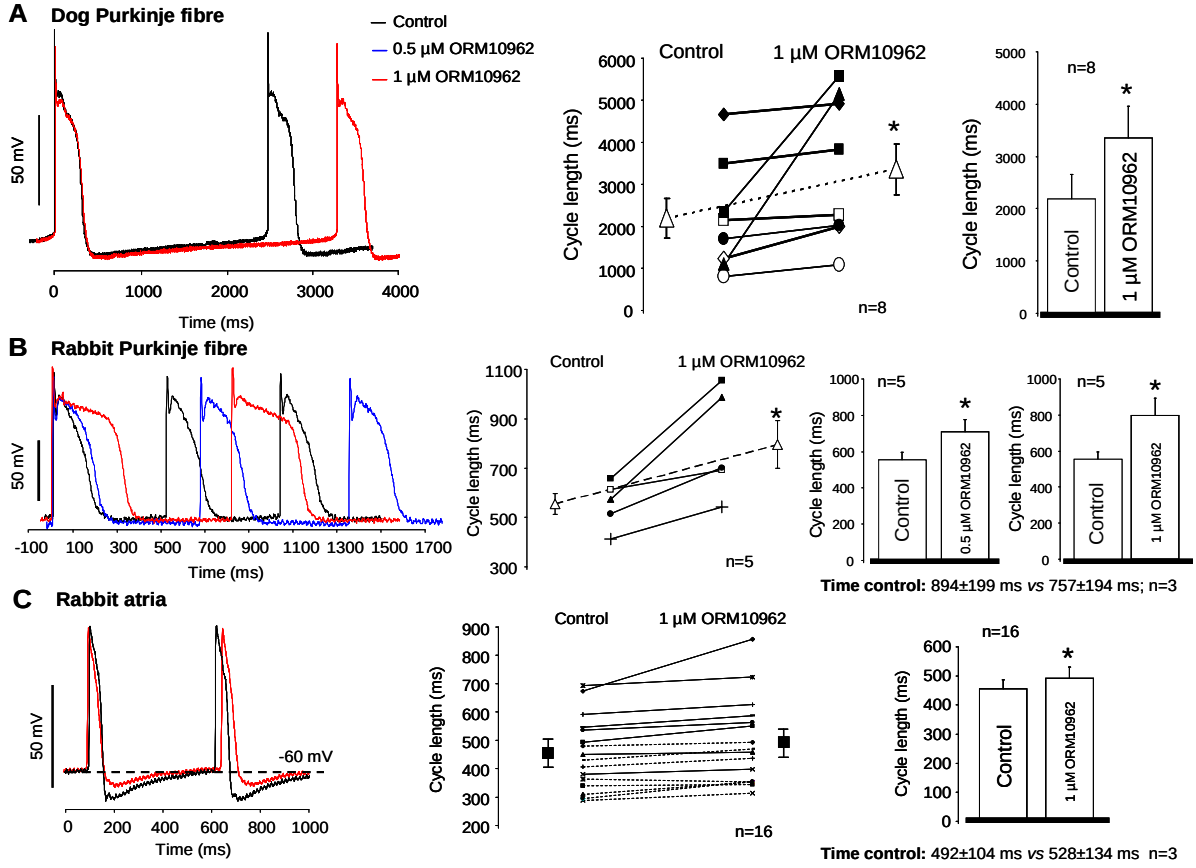

Figure 16. Effect of selective NCX inhibition by 0.5 and 1 µM ORM-10962 on the cycle length of spontaneous action potentials recorded from dog Purkinje fibres (Panel A), rabbit Purkinje fibres (Panel B) and from rabbit atrial (Panel C) samples. *Left panels show original spontaneous AP waveforms in control conditions and after application of ORM-10962. Scatter diagrams (middle) as well as bar diagrams (right) illustrate the effects of ORM-10962 in dog Purkinje fibres (A), rabbit Purkinje fibres (B) and in rabbit atrial (C) samples. Results of individual experiments are also shown in scatter diagrams (middle). Open triangles indicate the mean values of cycle length in control conditions and in the presence of ORM-10962. Values are means ± SEM, $p<0.05$.*

The selective NCX inhibition by ORM-10962 was investigated on the spontaneous automaticity in dog and rabbit right ventricular Purkinje fibres, as well as in rabbit right atrial reparations.

In dog Purkinje fibres (**Figure 16.A**) 1 µM ORM-10962 exerted clear lengthening effect on the cycle length of 8/8 spontaneous action potentials (2094.7±399 ms *vs* 3358.7±607 ms*; n=8/8 hearts, $p<0.05$).

In rabbit Purkinje fibres (**Figure 16.B**) we observed significant cycle lengthening effect of spontaneous action potentials after application of 0.5 µM (554.5±42.4 ms *vs* 708.2±68.3 ms*; n=5/5 hearts, $p<0.05$) and 1 µM ORM-10962 (554.5±42.4 ms *vs* 795.8±96.6 ms*, n=5/5 hearts, $p<0.05$). In rabbit atrial measurements (**Figure 16.C**), following application of 1 µM ORM-10962 moderate but significant lengthening effect on the cycle length was observed (455.1±32 ms *vs* 493.0±39 ms*, $p<0.05$, n=16/16 hearts). The corresponding time control measurements exerted no effect after application of the vehicle of ORM-10962 (DMSO).

3.7.2. Effect of NCX inhibition on spontaneous automaticity after ivabradine treatment

In this set of experiments 3 µM ivabradine was applied on rabbit right atrial tissue strips to reduce spontaneous frequency. Under control condition the cycle length was 419.1±36.1 ms which increased to 574.9±65 ms after application of 3 µM ivabradine (Δ= 25.9±6.1%*, n=5/5, $p<0.05$). 1 µM ORM-10962 caused further statistically significant increase in cycle length: 702.4±92.2 ms (Δ=21.2±4.7 %*, n=5/5, $p<0.05$; **Figures 17. A-B**). As **Figure 17. C** summarizes the ORM-induced increase in the cycle length after application of ivabradine was significantly larger compared with the ORM application alone (21.2±4.7 % *vs* 8.9±3.4%*). During time control experiments we found similar effect of ivabradine compared with control (440±49 ms *vs* 620±92* ms, n=3, $p<0.05$), but the subsequently applied vehicle (DMSO) failed to influence the cycle length (656±110 ms, n=3).

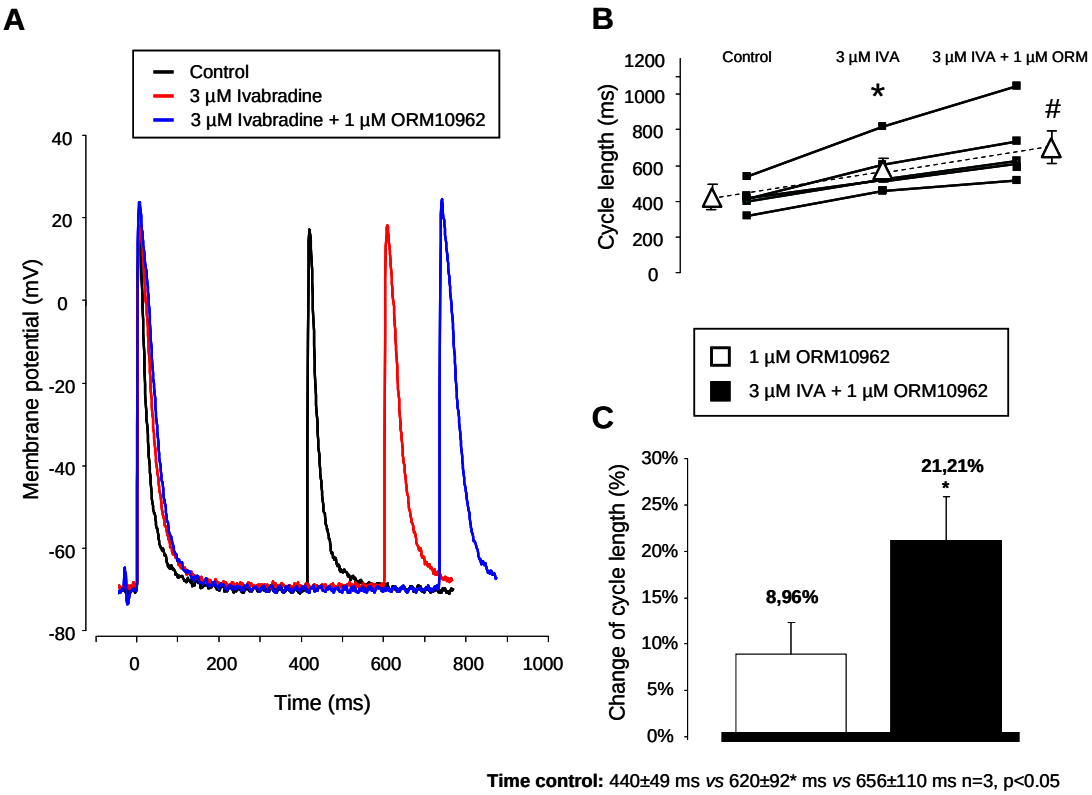

Time control: 440±49 ms *vs* 620±92* ms *vs* 656±110 ms n=3, p<0.05

Figure 17. Application of 3 µM ivabradine considerably increased the ORM-10962 induced reduction in spontaneous action potential firing in spontaneously beating rabbit atrial tissue. Panel A. *shows original spontaneous AP waveforms in control conditions, after application of 3 µM ivabradine and subsequently applied 1 µM ORM-10962.* **Panel B.** *Scatter diagram illustrates the individual experiments as well as the mean values (the open triangles), n=5, p<0.05.* **Panel C.** *Bar diagrams summarize the ORM-induced reduction of spontaneous AP firing frequency alone and with 3 µM ivabradine + 1 µM ORM-10962 administration. Values are means ± SEM, n=5, p<0.05. The parallel measured time control showed similar effect of ivabradine, which was previously observed, however the subsequently applied vehicle failed to influence the cycle length, n=3.*

3.8. The antiarrhythmic effect of selective NCX inhibition on delayed afterdepolarizations *in vitro*

This experiment was designed to investigate the effect of ORM-10962 on delayed (DAD) afterdepolarizations in dog cardiac Purkinje fibres applying the conventional microelectrode technique. DAD was evoked by 150 nM digoxin, which is a well-known Na^+/K^+ pump inhibitor. After 40 stimuli train with a cycle length of 400 ms, several DAD's were observed during the stimulation-free period (**Figure 18. A** left and mid panels). Further addition of 1 µM ORM-10962 significantly decreased the DAD's amplitude (from 5.3±0.7 mV to 1.5±0.3 mV; n=8, p<0.05; **Figure 18. A** right panel).

In some of these experiments digoxin evoked a run of extra beats (cellular, corresponding to the *in vivo* extrasystole) after the termination of the stimulus train, which could be successfully abolished by the application of 1 μM ORM-10962 (**Figure 18. B**).

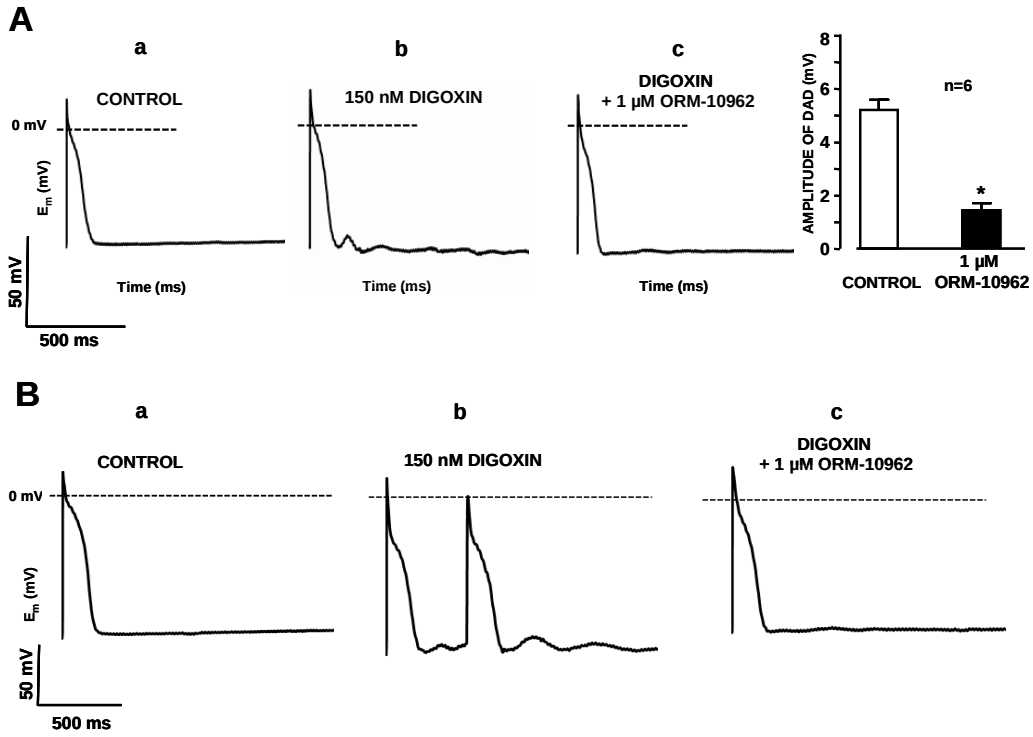

Figure 18. The effect of 1 μM ORM-10962 on the DAD amplitude in canine right ventricular Purkinje fibres. Panel A. *DAD's were evoked by a 40 stimuli train with a stimulation cycle length of 400 ms in the presence of 150 nM digoxin. Trace a) is control recording, trace b) indicates the induction of DAD by 150 nM digoxin, and trace c) demonstrates that 1 μM ORM-10962 significantly decreases DAD amplitudes in the continuous presence of digoxin. Diagram depicts the effects of 1 μM ORM-10962 on the amplitude of DAD. Bars represent means ± SEM, *p<0.05.* **Panel B.** *Representative measurement when spontaneous activity was recorded after a 40 stimuli train with a stimulation cycle length of 400 ms in the presence of 150 nM digoxin (trace b). Application of 1 μM ORM-10962 in the presence of digoxin completely abolished the spontaneous activity (trace c).*

3.9. Effect of selective NCX inhibition on Ca^{2+} transient and action potentials when forward or reverse mode is facilitated

The previous experiment (**Figure 18.**) suggests antiarrhythmic effect of selective NCX inhibition. Theoretically inhibition of both modes of NCX could reduce the DAD incidence: inhibition of reverse mode may reduce the intracellular Ca^{2+} level while inhibition of forward mode may decrease the amplitude of DAD's. Since under Na^+/K^+ pump inhibition both mode

of NCX may be activated by the high $[Na^+]_i$ and $[Ca^{2+}]$ levels we attempted to model this setting by facilitation of both mode of NCX.

In the first set of experiment extracellular Na^+ concentration was decreased to 70 mM, while the solution was supplemented with 70 mM choline-cloride thus the lower electrochemical driving force for Na^+ stimulates the reverse mode of NCX. In these measurements NCX inhibition with 1µM ORM-10962 slightly, but significantly lengthened the repolarization of action potentials (APD_{90}= 184±10.4 ms *vs* 205±7.3 ms*; APD_{75}=171.7±10.9 ms *vs* 192.7±7.8 ms*, APD_{50}= 148±10 ms *vs* 169±8.3 ms*; APD_{25}=104.9±8.4 ms *vs* 121±10.7 ms*; n=6, p<0.05 **Figure 19. A**). The CaT and cell shortening increased by the administration of low Na^+-Tyrode's (not shown), and significantly decreased when 1 µM ORM-10962 was applied (**Figure 19. B)** CaTs under control condition: 8.47±0.83 AU → low Na^+: 11.53±2.50 AU → 1 µM ORM-10962: 9.46±1.98 AU*; n=5, p<0.05. The transient amplitude decrease after ORM-10962 application was -16.07±5.77%*. The results of cell shortening measurements were the following: control: -3.80±1.4 AU → low Na^+: -6.61±2.18 AU → 1 µM ORM-10962: -4.01±1.79 AU*; n=5, p<0.05. The decrease of cell shortening was -38.12±16.45%* after ORM-10962 application. The diastolic Ca^{2+} significantly decreased after ORM-10962 application (*vs* low Na^+): 31.8±3.9 AU *vs* 28.6±2.9 AU*; n=5, p<0.05.

In another set of experiment enhanced NCX forward mode was achieved by 1 µM forskolin which increases the intracellular Ca^{2+} level through protein-kinase mediated phosphorylation of the I_{CaL}. The plateau voltage of the action potential was significantly depressed after application of 1µM ORM-10962 ($plateau_{50}$= 9.7±2.2 mV *vs* 3.7±2.9 mV*; n=6, p<0.05 *vs* forskolin) without consistently changing phase 3 repolarization (**Figure 20. A**). Application of 600 nM forskolin in single ventricular dog myocytes increased the amplitude of transient and cell shortening. Application of 1 µM ORM-10962 increased further the amplitudes significantly (**Figure 20. B**). CaTs under control condition: 15.89±1.82 AU → 600 nM forskolin: 13.72±1.50 AU → 1 µM ORM-10962: 16.21±1.80 AU*; n=5, p<0.05. The increase of transient amplitude was 18.3±3.13%* after ORM-10962 application. Cell shortening under control condition: -2.56±0.49 AU → 600 nM forskolin: -3.64±0.81 AU → 1 µM ORM-10962: -5.43±1.14 AU*; n=5, p<0.05. The increase of cell shortening amplitude was 56.47±17.85%* after ORM-10962 application. The diastolic Ca^{2+} did not change significantly during the experiment (data not shown).

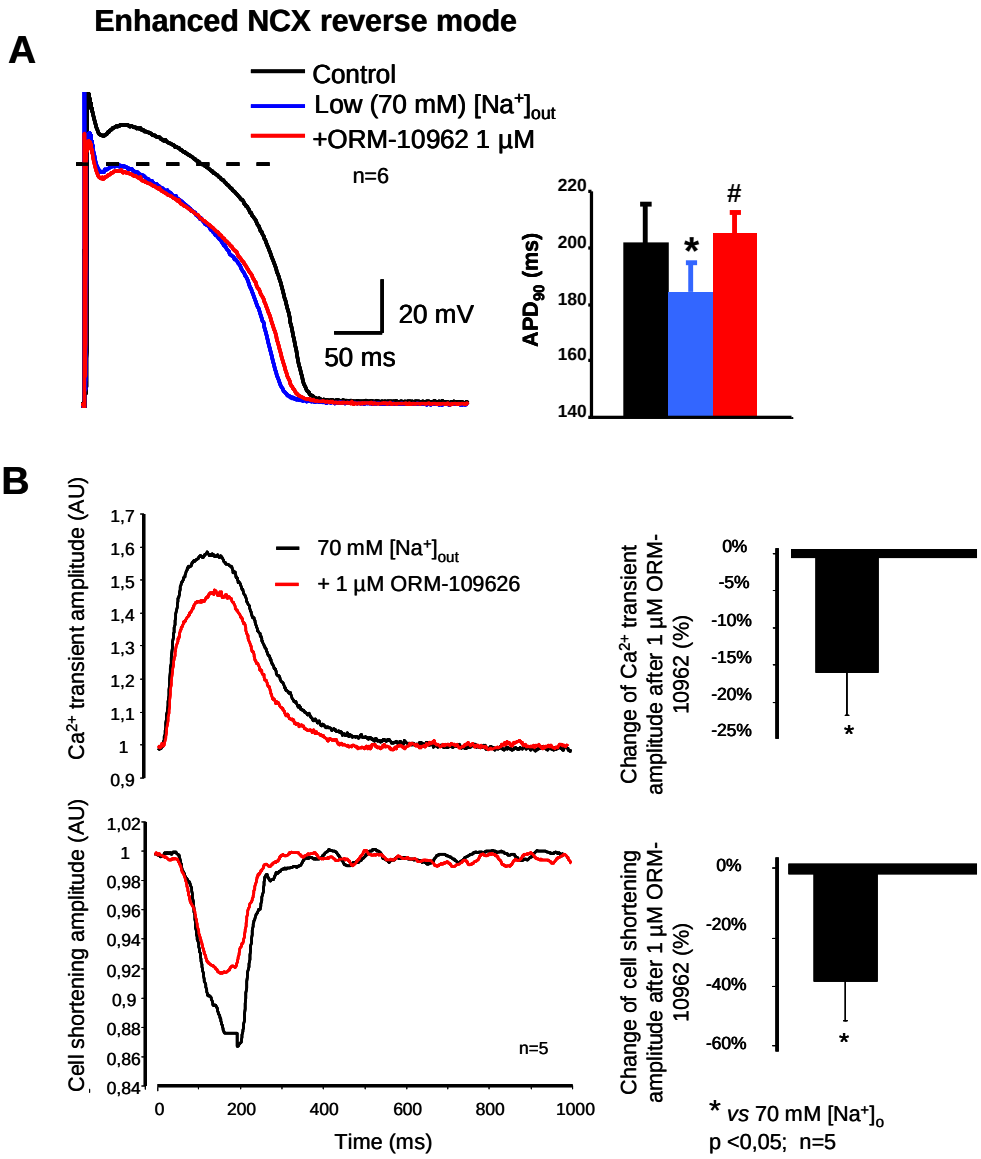

Figure 19. Effects of NCX inhibition during enhanced NXC reverse mode. Panel A. *AP was recorded from papillary muscles in low Na^+ (70 mM) solution, when the reverse mode of NCX was facilitated. The stimulation frequency was 1 Hz. The bars represent APD_{90}, $p<0.05$ control vs low $[Na^+]_{out}$, # =$p<0.05$ low $[Na^+]$out, vs ORM-10962 1µM, n=6.* **Panel B.** *shows representative CaT and cell shortening measurement when NCX reverse mode was facilitated by 70 mM $[Na^+]_{out}$ reduction in dog left ventricular myocytes. 1µM ORM-10962 significantly decreased the amplitudes of the CaT and cell shortening (red lines). The changes are depicted by bar graphs, values are means ± SEM.*

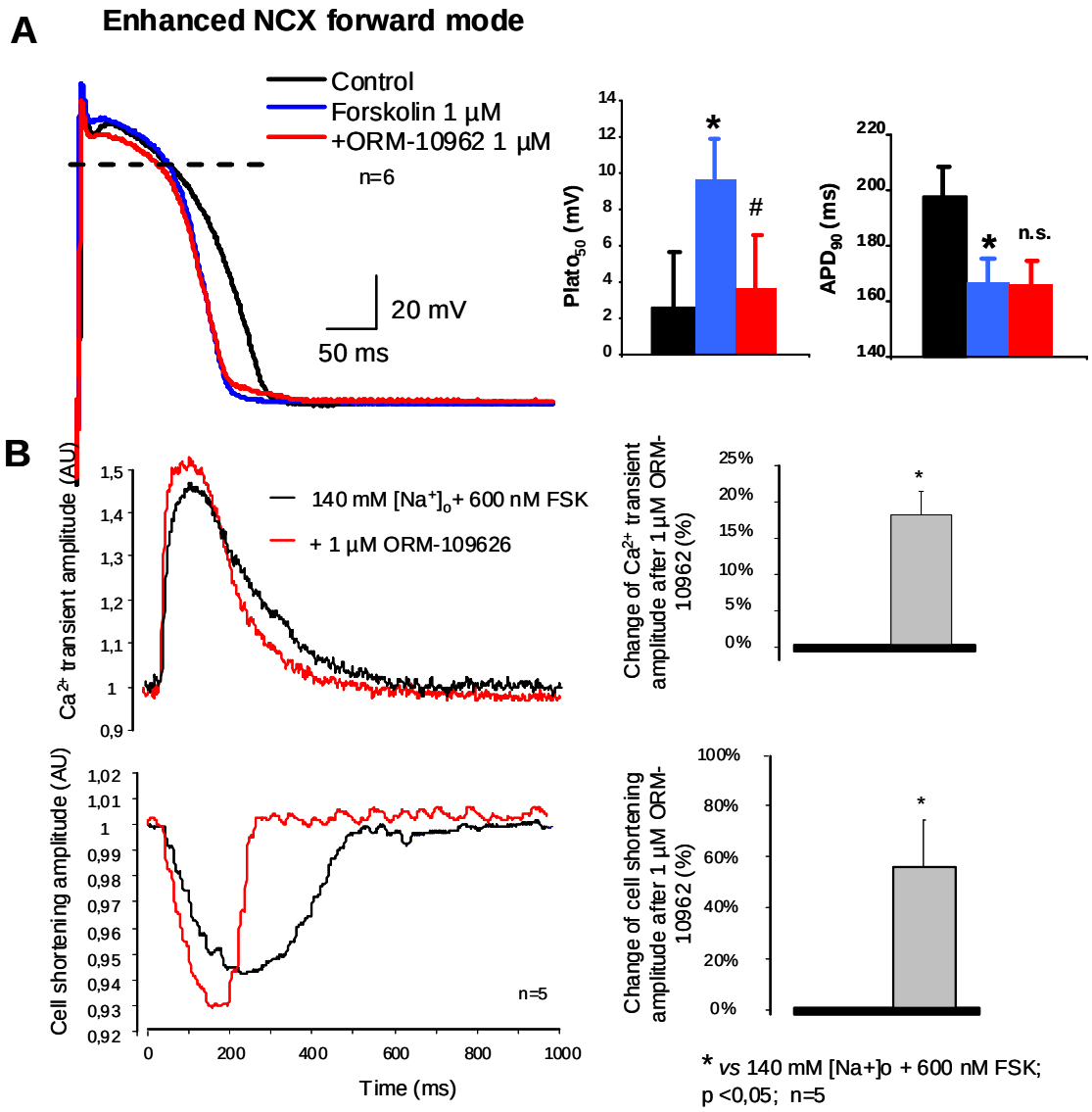

Figure 20. Effect of NCX inhibition during enhanced NCX forward mode. Panel A. *AP was measured from papillary muscle in the presence of 1 µM forskolin, when the forward mode of NCX was enhanced. The plateau potential was significantly suppressed without change of APD_{90}. The stimulation frequency was 1 Hz. The bars represent plateau potential at 50% repolarization time and action potential duration at 90% repolarization time, p<0.05 control vs forskolin, # =p<0.05 forskolin vs 1µM ORM-10962, n=6.* **Panel B**. *shows representative CaT and cell shortening measurements when NCX forward mode was facilitated by 600 nM forskolin in dog left ventricular myocytes. 1µM ORM-10962 significantly increased the amplitudes of the CaT and cell shortening (red lines). The changes are depicted by bar graphs, values are means ± SEM.*

4. DISCUSSION

The pivotal role of NCX in the physiological Ca^{2+} handling as well as in several types of arrhythmias is strongly suggested based on experimental and computation modelling studies (20, 21, 23, 74-77). Furthermore, the possible contribution of NCX to pacemaker activity was also claimed in several studies (33-37). However, the lack of appropriate selectivity of the applied NCX inhibitors has made the data interpretation difficult and some important points are not fully clarified. The inotropic effect of selective NCX inhibition was expected however many studies reported lack of effect after selective NCX inhibition (28, 30, 31, 78). Indeed, these compounds influenced the I_{CaL} in some extent suggesting some reduction in the Ca^{2+} influx which may counterbalance the inotropic effect. Many studies claimed marked antiarrhythmic effect of selective NCX inhibition however the exact mechanism of the effect could also not been clarified because of the lack inhibitor without major influence on I_{CaL}.

Recently we had a possibility to characterize two novel NCX inhibitors, ORM-10103 and ORM-10962. In this thesis we summarize that these compounds in addition of strong potency to suppress the NCX current, they exerted improved selectivity, i.e. without influence on the I_{CaL}. Our results with the novel compound ORM-10962 revealed moderate positive inotropic effect of selective NCX inhibition and supported the previous hypothesis suggesting important role of NCX in spontaneous pacemaker activity. Furthermore, our data provide evidence regarding the role of reverse mode inhibition against Na^{+} induced Ca^{2+} load mediated arrhythmias. Therefore, ORM-10962 may provide a new, appropriate tool for NCX investigations and selective NCX inhibition could be considered as a novel promising antiarrhythmic strategy.

4.1. ORM-10962 exerted improved efficacy and specificity in comparison with ORM-10103

Previously, the most successfully used NCX inhibitors like KB-R7943 and SEA0400 considerably improved our knowledge about the role of NCX regarding the electromechanical coupling and arrhythmogenesis (55, 79-83), but these inhibitors were not appropriately selective *i.e.* certain amount of I_{CaL} and I_K currents contaminated the results making the data

interpretation difficult. Therefore, the most important requirement for a NCX inhibitor – beyond potent blocking of NCX – is a minimal influence on the I_{CaL} current. In previous studies of our laboratory (10, 28, 55, 83, 84), we reported that ORM-10103 effectively (**Figure 7.**) and selectively inhibits NCX in dog ventricular myocytes without influencing the I_{CaL} current (figure not shown). Furthermore it was effective against triggered arrhythmias, namely it clearly decreased the amplitude of pharmacologically induced EAD and reduced the DAD incidence. However, this compound had 25.4% blocking effect on I_{Kr} at close to the maximal NCX inhibition concentration range (**Figure 13.**). Therefore, this compound has some limitations in studying the role of NCX since it also influences the ventricular repolarization. The improved compound, ORM-10962 has no effect on I_{CaL} even in higher concentration (1 µM) (**Figure 9.**) as well as it does not influence the peak and late sodium currents and the N^+/K^+ pump (**Figure 10.)**, and the main repolarizing potassium currents like I_{K1}, I_{to}, I_{Kr} and I_{Ks} (**Figures 11.** and **13**), at close the maximal NCX inhibition (~80%) concentration range. Furthermore, it has much less EC_{50} values (55/67 nM for inward/outward NCX currents, respectively) at both modes of NCX (**Figure 8.)**. The better selectivity and improved efficacy of ORM-10962 account for performing the further experiments with ORM-10962.

4.2. Selective NCX inhibition has a moderate positive inotropic effect without major influence on the action potential under normal condition

It is widely accepted that the NCX operates primarily in forward mode during a normal AP (76, 77), therefore, when inhibited, intracellular Ca^{2+} load, and AP shortening is expected. However, our laboratory and others failed to find any influence of SEA0400 and ORM-10103 on AP and CaT (28-31, 78, 85). In contrast, we observed a marginal but significant increase on CaT and cell shortening after application of ORM-10962 in dog ventricular myocytes (**Figure 14.**). Thus, our results support the hypothesis regarding the positive inotropic effect of selective NCX inhibition; however, the relatively small extent of the effect is unexpected and unclear. A possible explanation could be the concomitant inhibition of reverse mode activity, which simultaneously decreases the intracellular Ca^{2+} influx. Further possibility could be the PMCA which may also contribute to Ca^{2+} extrusion (86) and therefore it may compensate for the reduced NCX function. Based on our previous study (28), where the NCX was measured in the presence of intact Ca^{2+} cycle, we proposed that under normal condition, the inward NCX current has relatively low amplitude thus the

inhibition of this small current may be fully compensated by the above mentioned mechanisms.

The effect of ORM-10962 on AP was investigated in multicellular preparations from different transmural regions and showed tissue specific changes (**Figure 15.**). The selective NCX inhibition marginally increased the APD_{90} in epicardial tissue without significant influence on subendocardial region and in Purkinje fibres. In healthy myocardium the cells are well coupled electrically, and this electronic interaction largely minimizes the repolarization changes at tissue level, while these alterations could be augmented at cellular level which may explain the marginal effect in epicardial tissue (4). Previous studies (28, 77) seem to support our suggestion that under normal condition only small net NCX current is evoked during the AP and the influence of the inhibition of this small current may be compensated for by the repolarization reserve (9). The momentary magnitude of NCX current under the AP depends on the actual voltage, intracellular Na^+ and Ca^{2+} levels. The kinetics of the APs, CaTs may differ regarding the tissue type (subendocardial, subepicardial, Purkinje fibre) and could be different from cell to cell obtained from the same heart region. We cannot rule out the possibility that the net current of the NCX is changing throughout the ventricular wall: it becomes inward from epi- to endocardial tissue.

4.3. Selective NCX inhibition decreases the spontaneous pacing rate of SA node and Purkinje fibres under normal conditions

We found significant negative chronotropic effect of ORM-10962 in the SA node and Purkinje fibres (**Figure 16.**). Previous studies showed that two competing mechanisms may play a role during the initiation of each heartbeat: one is the M (membrane voltage) clock (33, 34) claiming pivotal role of I_f in determining the actual frequency, and the second one is the Ca^{2+} clock. According to the Ca^{2+} clock hypothesis, the local Ca^{2+} release from the SR causes local depolarization, which enhances the NCX forward activity. Forward NCX due to Ca^{2+} extrusion generate depolarizing Na^+ influx, thus may contribute to the gradual depolarization initiated by the I_f pacemaker current. Our results seem to be in line with this hypothesis, since NCX inhibition by ORM-10962 decreased the spontaneous firing rate in both canine and rabbit Purkinje-fibres as well as in rabbit atrial tissue samples (**Figure 16.**).Therefore, NCX inhibition may suppress the spontaneous diastolic depolarization and increase the cycle length of the pacemaker cells, without directly influencing the I_f (**Figure 12.**). However, considering

these marginal but statistically significant effect of ORM-10962, we assume that the NCX may have only a small modulatory role in diastolic depolarization.

The current theory synthesizes the M-clock and Ca-clock mechanisms, claiming Ca^{2+}-clock together with M-clock form a coupled-clock system where neither clock is dominant; instead, together they control the spontaneous AP firing frequency and rhythm in the pacemaker cells (36, 37). These studies showed that ivabradine, however inhibits selectively the I_f current, it also indirectly suppresses Ca^{2+} cycling by reducing SR Ca^{2+} load, without direct influence on the ion channels (I_{Ca}, RyR) of the Ca^{2+} handling. These results may indicate that the bradycardia occurred by ivabradine is not only the consequence of the I_f blockade alone, but it is rather due to the perturbation of the crosstalk within the coupled-clock system (36). The underlying mechanism may be the reduction in SR load, which leads to prolonged local Ca^{2+} release period, causing reduced and delayed NCX function in the membrane clock. Our results may support this crosstalk theory since the AP firing frequency of the ivabradine pre-treated spontaneous rabbit atria was further reduced after application of ORM-10962 (**Figure 17.**).

4.4. NCX inhibition is effective against Na^+ induced Ca^{2+} load mediated delayed afterdepolarizations

Previous studies with SEA0400 and ORM-10103 suggested that NCX inhibition could be effective against Na^+ induced Ca^{2+} load mediated DADs (28, 44, 60, 63, 65, 87-90). The afterdepolarizations were evoked by inhibition of Na^+/K^+ pump by glycosides, leading to accumulation in $[Na^+]_i$ and AP shortening (91). The elevated intracellular Na^+ level induces increased reverse NCX activity causing marked gain in intracellular Ca^{2+} and consequently in the SR Ca^{2+} level (92). Selective NCX inhibition by applying ORM-10962 completely abolished the digoxin induced spontaneous automaticity and significantly decreased DADs amplitude (**Figure 18.**). Similar results were observed by application of ORM-10103 (10, 27, 28), where not only DAD, but also EAD amplitudes reduced significantly after the ORM-10103 treatment, however this compound is not completely selective for NCX (**Figure 13.C**).

The underlying mechanism of the effect is not exactly clarified. During Na^+ induced Ca^{2+} load both modes of the NCX is facilitated by the increased level of the Na^+ and Ca^{2+} ions. Therefore, theoretically inhibition of both modes could be antiarrhythmic since

suppression of the reverse mode may decrease the intracellular Ca^{2+}, while inhibition of forward mode may directly reduce the amplitude and incidence of DAD's amplitude. In order to address this question we attempted to selectively facilitate the reverse (**Figure 19.)** and forward (**Figure 20.**) mode NCX activity.

In the presence of low Na^{+} containing Tyrode's solution, clear negative inotropic effect could be observed after application of ORM-10962 suggesting a decrease in $[Ca^{2+}]_i$ level. Furthermore, the APD was marginally but statistically significantly lengthened which may also indicate increased reverse mode activity and consequently larger outward current (**Figure 19.A**). This result may also suggest that during Na^{+} induced Ca^{2+} load the NCX operates mainly in reverse mode therefore its inhibition resulted in net loss of intracellular Ca^{2+} and negative inotropy. Similar results were obtained with ORM-10103 in our previous study (28).

In a separate experiment the forward mode was facilitated by forskolin which increases the intracellular Ca^{2+} level via adenylate-cyclase activation. Under this setting the selective NCX inhibition caused net gain in intracellular Ca^{2+} and positive inotropy as well as slight depression in the AP plateau potential (**Figure 20.A**). The positive inotropy can be explained by the shift of the NCX reverse potential caused by increased intracellular Ca^{2+} which may result in shift to the positive potentials facilitating ion transport in the forward mode. The inhibition of the NCX may reduce the rate of the Ca^{2+} extrusion with a concomitant compensatory reduction of the I_{CaL} (the Ca^{2+} influx and efflux must be equal) achieved by the increased Ca^{2+} transient. This shift in current balance may account (at least partially) for the depressed plateau level of the action potential.

Summarizing these results we suggest that during Na^{+} induced Ca^{2+} load both modes of the NCX is facilitated but the reverse mode may be predominant during this condition. Inhibition of both modes could be theoretically antiarrhythmic. However, the inhibition of the reverse mode may have more importance since the net loss of the intracellular Ca^{2+} may indirectly reduce the forward mode activity and *per se* reduces the DAD amplitude and incidence.

5. CONLUSIONS AND POTENTIAL SIGNIFICANCE

1) We have shown that two newly synthesized NCX inhibitors, ORM-10103 and ORM-10962, effectively inhibit both modes of the NCX current. ORM-10962 is more potent than the previously described ORM-10103, having the EC_{50} value of the ORM-10962 in the nanomolar range.
2) ORM-10962 was found a highly selective NCX inhibitor, because even a higher concentration (1μM) did not influence other transmembrane ionic currents in the heart (I_{CaL}, I_{NaL}, $I_{Na\ peak}$, Na^+/K^+ pump, I_{Kr}, I_{Ks}, I_{to}, I_{K1}, I_f). However, the ORM-10103 in a higher concentration (10 μM) has a moderated I_{Kr} blocking effect.
3) Selective NCX inhibition by ORM-10962 exerted a marginal positive inotropic effect as shown by CaT and cell shortening measurements. In the same time, it failed to influence the ventricular AP under normal condition.
4) In line with previous hypothesis, we have demonstrated experimentally that NCX has a role in the pacemaking mechanisms. The NCX inhibition significantly prolongs the cycle length of spontaneous APs recorded from dog and rabbit Purkinje fibres and atrial samples. Moreover, addition of ORM-10962 after ivabradine application a further reduction in the spontaneous AP firing frequency was observed which may support the coupled-clock hypothesis.
5) NCX inhibition completely abolished the digoxin-induced automaticity and significantly decreased the amplitude of DAD's. The underlying mechanism was addressed by investigating the shifts in the balance of the forward and reverse modes of NCX. When forward mode was facilitated, NCX inhibition caused a significant positive inotropic effect without major change in APD, however in those experiments in which reverse mode was enhanced negative inotropic effect was observed, with APD lengthening. We conclude that under Na^+ induced Ca^{2+} load the reverse mode became predominant therefore the subsequently applied NCX inhibition decreases the Ca^{2+} transient amplitude. In line with this, we suggest that during digoxin-induced DADs, where also Na^+ induced Ca^{2+} load occurred, the inhibition of the facilitated reverse mode may have more importance in the development of antiarrhythmic effect.

6. ACKNOWLEDGEMENTS

I am very grateful to **Professor Julius Gy. Papp MD, DSc, academian**, for his continuous support, his kindness, inspirational comments and constructive criticism, his suggestions which were always of help and are greatly appreciated. Also, to **Professor András Varró MD, DSc** for providing me the opportunity for research as PhD student at the Department of Pharmacology and Pharmacotherapy, University of Szeged and for the helpful discussions which were exceptionally useful during my work.

I am especially thankful to my PhD supervisor **Dr. Norbert Jost**, for personal guidance, continuous support of my work and for introducing me to the fascinating world of cardiac cellular electrophysiology.

My husband, **Dr. Norbert Nagy** sincerely thanked for the excellent collaboration during the years, for the many hours of splendid discussions and helpful scientific lessons. Without his continuous support and optimistic attitude to the scientific problems, this PhD study could have hardly come to an end.

I wish to thank my senior colleague, **Dr. László Virág** and my PhD student colleagues **Attila Kristóf**, **András Horváth**, **Claudia Corici** and **Amir Geramipour** for their continuous support and help in my work, for creating a cheerful and social milieu in the laboratory, and to **Mrs. Zsuzsanna Molnár**, **Mr. Gábor Dobai** and **Mr. Gábor Girst** for their helpful technical assistance. I am also grateful to **Dr. Károly Acsai** and **Dr. Balázs Ördög** for inspiring discussions and lots of excellent advices.

I also wish to thank my parents (**Gizella** and **Tibor**) and my younger sister (**Sára**) and brother (**Gergely**) for their endless love, trust and support.

I am also thankful to my dear friends (especially to **Dr. Karolina Somogyi** and **Dr. Zsolt Somogyi**) for their support and encouragement.

This work was supported by the grants from the National Research Development and Innovation Office (OTKA NN-109994, NK-104331, K-119992, GINOP-2.3.2-15-2016-00006 and GINOP-2.3.2-15-2016-00012), the National Office for Research and Technology- Baross and Ányos Jedlik Programmes (REG-DA-09-2-2009-0115-NCXINHIB and NKFP_07_01-RYT07_AF) , the Ministry of National Education - New National Excellence Program of the Ministry of Human Capacities (UNKP-16-3-IKT/147-1787/8/2016-ÖSZT-95), HU-RO Cross-Border Cooperation Programmes (HURO/1001/086/2.2.1_HURO-TWIN) and the Hungarian Academy of Sciences. I especially acknowledge the professional support offered by Orion Pharma Finnland by supplying ORM-10103 and ORM-10962 compounds.

7. REFERENCES

1 Nerbonne JM, Kass RS. Molecular physiology of cardiac repolarization. Physiol Rev 2005; 85: 1205-53.

2 Zicha S, Moss I, Allen B, et al. Molecular basis of species-specific expression of repolarizing K+ currents in the heart. American journal of physiology Heart and circulatory physiology 2003; 285: H1641-9.

3 Nerbonne JM, Guo W. Heterogeneous expression of voltage-gated potassium channels in the heart: roles in normal excitation and arrhythmias. Journal of cardiovascular electrophysiology 2002; 13: 406-9.

4 Antzelevitch C. Molecular basis for the transmural distribution of the transient outward current. The Journal of physiology 2001; 533: 1.

5 Allessie M, Ausma J, Schotten U. Electrical, contractile and structural remodeling during atrial fibrillation. Cardiovascular research 2002; 54: 230-46.

6 Boyden PA, Hirose M, Dun W. Cardiac Purkinje cells. Heart rhythm : the official journal of the Heart Rhythm Society; 7: 127-35.

7 Ravens U, Cerbai E. Role of potassium currents in cardiac arrhythmias. Europace : European pacing, arrhythmias, and cardiac electrophysiology : journal of the working groups on cardiac pacing, arrhythmias, and cardiac cellular electrophysiology of the European Society of Cardiology 2008; 10: 1133-7.

8 Roden DM. Taking the "idio" out of "idiosyncratic": predicting torsades de pointes. Pacing and clinical electrophysiology : PACE 1998; 21: 1029-34.

9 Biliczki P, Virag L, Iost N, Papp JG, Varro A. Interaction of different potassium channels in cardiac repolarization in dog ventricular preparations: role of repolarization reserve. British journal of pharmacology 2002; 137: 361-8.

10 Jost N, Nagy N, Corici C, et al. ORM-10103, a novel specific inhibitor of the Na+/Ca2+ exchanger, decreases early and delayed afterdepolarizations in the canine heart. British journal of pharmacology 2013; 170: 768-78.

11 Jost N, Virag L, Bitay M, et al. Restricting excessive cardiac action potential and QT prolongation: a vital role for IKs in human ventricular muscle. Circulation 2005; 112: 1392-9.

12 Szabo G, Szentandrassy N, Biro T, et al. Asymmetrical distribution of ion channels in canine and human left-ventricular wall: epicardium versus midmyocardium. Pflugers Archiv : European journal of physiology 2005; 450: 307-16.

13 Lukas A, Antzelevitch C. Differences in the electrophysiological response of canine ventricular epicardium and endocardium to ischemia. Role of the transient outward current. Circulation 1993; 88: 2903-15.

14 Xiong W, Tian Y, DiSilvestre D, Tomaselli GF. Transmural heterogeneity of Na+-Ca2+ exchange: evidence for differential expression in normal and failing hearts. Circulation research 2005; 97: 207-9.

15 Nicoll DA, Longoni S, Philipson KD. Molecular cloning and functional expression of the cardiac sarcolemmal Na(+)-Ca2+ exchanger. Science (New York, NY) 1990; 250: 562-5.

16 Lytton J. Na+/Ca2+ exchangers: three mammalian gene families control Ca2+ transport. The Biochemical journal 2007; 406: 365-82.

17 Despa S, Brette F, Orchard CH, Bers DM. Na/Ca exchange and Na/K-ATPase function are equally concentrated in transverse tubules of rat ventricular myocytes. Biophysical journal 2003; 85: 3388-96.

18 Sher AA, Noble PJ, Hinch R, Gavaghan DJ, Noble D. The role of the Na+/Ca2+ exchangers in Ca2+ dynamics in ventricular myocytes. Progress in biophysics and molecular biology 2008; 96: 377-98.
19 McDonald RL, Colyer J, Harrison SM. Quantitative analysis of Na+-Ca2+ exchanger expression in guinea-pig heart. Eur J Biochem 2000; 267: 5142-8.
20 Bers DM, Ziolo MT. When is cAMP not cAMP? Effects of compartmentalization. Circulation research 2001; 89: 373-5.
21 Bers DM. Calcium cycling and signaling in cardiac myocytes. Annual review of physiology 2008; 70: 23-49.
22 Bers DM. Altered cardiac myocyte Ca regulation in heart failure. Physiology (Bethesda, Md) 2006; 21: 380-7.
23 Bers DM. Cardiac Na/Ca exchange function in rabbit, mouse and man: what's the difference? Journal of molecular and cellular cardiology 2002; 34: 369-73.
24 Choi HS, Eisner DA. The role of sarcolemmal Ca2+-ATPase in the regulation of resting calcium concentration in rat ventricular myocytes. The Journal of physiology 1999; 515 (Pt 1): 109-18.
25 Birinyi P, Acsai K, Banyasz T, et al. Effects of SEA0400 and KB-R7943 on Na+/Ca2+ exchange current and L-type Ca2+ current in canine ventricular cardiomyocytes. Naunyn-Schmiedeberg's archives of pharmacology 2005; 372: 63-70.
26 Kohajda Z, Farkas-Morvay N, Jost N, et al. The Effect of a Novel Highly Selective Inhibitor of the Sodium/Calcium Exchanger (NCX) on Cardiac Arrhythmias in In Vitro and In Vivo Experiments. PloS one 2016; 11: e0166041.
27 Banyasz T, Horvath B, Jian Z, Izu LT, Chen-Izu Y. Profile of L-type Ca(2+) current and Na(+)/Ca(2+) exchange current during cardiac action potential in ventricular myocytes. Heart rhythm : the official journal of the Heart Rhythm Society 2012; 9: 134-42.
28 Nagy N, Kormos A, Kohajda Z, et al. Selective Na /Ca exchanger inhibition prevents Ca overload induced triggered arrhythmias. British journal of pharmacology 2014.
29 Acsai K, Kun A, Farkas AS, et al. Effect of partial blockade of the Na(+)/Ca(2+)-exchanger on Ca(2+) handling in isolated rat ventricular myocytes. European journal of pharmacology 2007; 576: 1-6.
30 Farkas AS, Acsai K, Nagy N, et al. Na(+)/Ca(2+) exchanger inhibition exerts a positive inotropic effect in the rat heart, but fails to influence the contractility of the rabbit heart. British journal of pharmacology 2008; 154: 93-104.
31 Birinyi P, Toth A, Jona I, et al. The Na+/Ca2+ exchange blocker SEA0400 fails to enhance cytosolic Ca2+ transient and contractility in canine ventricular cardiomyocytes. Cardiovascular research 2008; 78: 476-84.
32 Farkas AS, Makra P, Csik N, et al. The role of the Na+/Ca2+ exchanger, I(Na) and I(CaL) in the genesis of dofetilide-induced torsades de pointes in isolated, AV-blocked rabbit hearts. British journal of pharmacology 2009; 156: 920-32.
33 Lakatta EG, DiFrancesco D. What keeps us ticking: a funny current, a calcium clock, or both? Journal of molecular and cellular cardiology 2009; 47: 157-70.
34 Lakatta EG. A paradigm shift for the heart's pacemaker. Heart rhythm : the official journal of the Heart Rhythm Society; 7: 559-64.
35 Yaniv Y, Lakatta EG. The end effector of circadian heart rate variation: the sinoatrial node pacemaker cell. BMB Rep 2015; 48: 677-84.
36 Yaniv Y, Sirenko S, Ziman BD, Spurgeon HA, Maltsev VA, Lakatta EG. New evidence for coupled clock regulation of the normal automaticity of sinoatrial nodal pacemaker cells: bradycardic effects of ivabradine are linked to suppression of

intracellular Ca(2)(+) cycling. Journal of molecular and cellular cardiology 2013; 62: 80-9.

37 Yaniv Y, Stern MD, Lakatta EG, Maltsev VA. Mechanisms of beat-to-beat regulation of cardiac pacemaker cell function by Ca(2)(+) cycling dynamics. Biophysical journal 2013; 105: 1551-61.

38 Monfredi O, Maltsev VA, Lakatta EG. Modern concepts concerning the origin of the heartbeat. Physiology (Bethesda, Md); 28: 74-92.

39 Sanders L, Rakovic S, Lowe M, Mattick PA, Terrar DA. Fundamental importance of Na+-Ca2+ exchange for the pacemaking mechanism in guinea-pig sino-atrial node. The Journal of physiology 2006; 571: 639-49.

40 Bogdanov KY, Vinogradova TM, Lakatta EG. Sinoatrial nodal cell ryanodine receptor and Na(+)-Ca(2+) exchanger: molecular partners in pacemaker regulation. Circulation research 2001; 88: 1254-8.

41 Herrmann S, Lipp P, Wiesen K, et al. The cardiac sodium-calcium exchanger NCX1 is a key player in the initiation and maintenance of a stable heart rhythm. Cardiovascular research; 99: 780-8.

42 Groenke S, Larson ED, Alber S, et al. Complete atrial-specific knockout of sodium-calcium exchange eliminates sinoatrial node pacemaker activity. PloS one; 8: e81633.

43 Antoons G, Willems R, Sipido KR. Alternative strategies in arrhythmia therapy: evaluation of Na/Ca exchange as an anti-arrhythmic target. Pharmacology & therapeutics 2012; 134: 26-42.

44 Takahashi K, Takahashi T, Suzuki T, et al. Protective effects of SEA0400, a novel and selective inhibitor of the Na+/Ca2+ exchanger, on myocardial ischemia-reperfusion injuries. European journal of pharmacology 2003; 458: 155-62.

45 Elias CL, Lukas A, Shurraw S, et al. Inhibition of Na+/Ca2+ exchange by KB-R7943: transport mode selectivity and antiarrhythmic consequences. American journal of physiology Heart and circulatory physiology 2001; 281: H1334-45.

46 Woodcock EA, Arthur JF, Harrison SN, Gao XM, Du XJ. Reperfusion-induced Ins(1,4,5)P(3) generation and arrhythmogenesis require activation of the Na(+)/Ca(2+) exchanger. Journal of molecular and cellular cardiology 2001; 33: 1861-9.

47 Yamamura K, Tani M, Hasegawa H, Gen W. Very low dose of the Na(+)/Ca(2+) exchange inhibitor, KB-R7943, protects ischemic reperfused aged Fischer 344 rat hearts: considerable strain difference in the sensitivity to KB-R7943. Cardiovascular research 2001; 52: 397-406.

48 Morita N, Lee JH, Bapat A, et al. Glycolytic inhibition causes spontaneous ventricular fibrillation in aged hearts. American journal of physiology Heart and circulatory physiology 2011; 301: H180-91.

49 Schafer C, Ladilov Y, Inserte J, et al. Role of the reverse mode of the Na+/Ca2+ exchanger in reoxygenation-induced cardiomyocyte injury. Cardiovascular research 2001; 51: 241-50.

50 Mukai M, Terada H, Sugiyama S, Satoh H, Hayashi H. Effects of a selective inhibitor of Na+/Ca2+ exchange, KB-R7943, on reoxygenation-induced injuries in guinea pig papillary muscles. Journal of cardiovascular pharmacology 2000; 35: 121-8.

51 Satoh H, Mukai M, Urushida T, Katoh H, Terada H, Hayashi H. Importance of Ca2+ influx by Na+/Ca2+ exchange under normal and sodium-loaded conditions in mammalian ventricles. Molecular and cellular biochemistry 2003; 242: 11-7.

52 Watano T, Harada Y, Harada K, Nishimura N. Effect of Na+/Ca2+ exchange inhibitor, KB-R7943 on ouabain-induced arrhythmias in guinea-pigs. British journal of pharmacology 1999; 127: 1846-50.

53 Wongcharoen W, Chen YC, Chen YJ, et al. Effects of a Na+/Ca2+ exchanger inhibitor on pulmonary vein electrical activity and ouabain-induced arrhythmogenicity. Cardiovascular research 2006; 70: 497-508.
54 Namekata I, Tsuneoka Y, Takahara A, et al. Involvement of the Na(+)/Ca(2+) exchanger in the automaticity of guinea-pig pulmonary vein myocardium as revealed by SEA0400. Journal of pharmacological sciences 2009; 110: 111-6.
55 Tanaka H, Shimada H, Namekata I, Kawanishi T, Iida-Tanaka N, Shigenobu K. Involvement of the Na+/Ca2+ exchanger in ouabain-induced inotropy and arrhythmogenesis in guinea-pig myocardium as revealed by SEA0400. Journal of pharmacological sciences 2007; 103: 241-6.
56 Nagy ZA, Virag L, Toth A, et al. Selective inhibition of sodium-calcium exchanger by SEA-0400 decreases early and delayed after depolarization in canine heart. British journal of pharmacology 2004; 143: 827-31.
57 Milberg P, Pott C, Fink M, et al. Inhibition of the Na+/Ca2+ exchanger suppresses torsades de pointes in an intact heart model of long QT syndrome-2 and long QT syndrome-3. Heart rhythm : the official journal of the Heart Rhythm Society 2008; 5: 1444-52.
58 Amran MS, Hashimoto K, Homma N. Effects of sodium-calcium exchange inhibitors, KB-R7943 and SEA0400, on aconitine-induced arrhythmias in guinea pigs in vivo, in vitro, and in computer simulation studies. The Journal of pharmacology and experimental therapeutics 2004; 310: 83-9.
59 Feng NC, Satoh H, Urushida T, et al. A selective inhibitor of Na+/Ca2+ exchanger, SEA0400, preserves cardiac function and high-energy phosphates against ischemia/reperfusion injury. Journal of cardiovascular pharmacology 2006; 47: 263-70.
60 Milberg P, Pott C, Frommeyer G, et al. Acute inhibition of the Na(+)/Ca(2+) exchanger reduces proarrhythmia in an experimental model of chronic heart failure. Heart rhythm : the official journal of the Heart Rhythm Society 2012; 9: 570-8.
61 Iwamoto T, Watanabe Y, Kita S, Blaustein MP. Na+/Ca2+ exchange inhibitors: a new class of calcium regulators. Cardiovascular & hematological disorders drug targets 2007; 7: 188-98.
62 Watano T, Kimura J, Morita T, Nakanishi H. A novel antagonist, No. 7943, of the Na+/Ca2+ exchange current in guinea-pig cardiac ventricular cells. British journal of pharmacology 1996; 119: 555-63.
63 Matsuda T, Arakawa N, Takuma K, et al. SEA0400, a novel and selective inhibitor of the Na+-Ca2+ exchanger, attenuates reperfusion injury in the in vitro and in vivo cerebral ischemic models. The Journal of pharmacology and experimental therapeutics 2001; 298: 249-56.
64 Matsuda T, Koyama Y, Baba A. Functional proteins involved in regulation of intracellular Ca(2+) for drug development: pharmacology of SEA0400, a specific inhibitor of the Na(+)-Ca(2+) exchanger. Journal of pharmacological sciences 2005; 97: 339-43.
65 Iwamoto T. Forefront of Na+/Ca2+ exchanger studies: molecular pharmacology of Na+/Ca2+ exchange inhibitors. Journal of pharmacological sciences 2004; 96: 27-32.
66 Chin TK, Spitzer KW, Philipson KD, Bridge JH. The effect of exchanger inhibitory peptide (XIP) on sodium-calcium exchange current in guinea pig ventricular cells. Circulation research 1993; 72: 497-503.
67 Hobai IA, Maack C, O'Rourke B. Partial inhibition of sodium/calcium exchange restores cellular calcium handling in canine heart failure. Circulation research 2004; 95: 292-9.

68 Hobai IA, O'Rourke B. The potential of Na+/Ca2+ exchange blockers in the treatment of cardiac disease. Expert opinion on investigational drugs 2004; 13: 653-64.
69 Hobai IA, Khananshvili D, Levi AJ. The peptide "FRCRCFa", dialysed intracellularly, inhibits the Na/Ca exchange in rabbit ventricular myocytes with high affinity. Pflugers Archiv : European journal of physiology 1997; 433: 455-63.
70 Patton C, Thompson S, Epel D. Some precautions in using chelators to buffer metals in biological solutions. Cell calcium 2004; 35: 427-31.
71 Varga Z, Gurrola-Briones G, Papp F, et al. Vm24, a natural immunosuppressive peptide, potently and selectively blocks Kv1.3 potassium channels of human T cells. Molecular pharmacology 2012; 82: 372-82.
72 Verkerk AO, den Ruijter HM, Bourier J, et al. Dietary fish oil reduces pacemaker current and heart rate in rabbit. Heart rhythm : the official journal of the Heart Rhythm Society 2009; 6: 1485-92.
73 Sirenko SG, Maltsev VA, Yaniv Y, et al. Electrochemical Na+ and Ca2+ gradients drive coupled-clock regulation of automaticity of isolated rabbit sinoatrial nodal pacemaker cells. American journal of physiology Heart and circulatory physiology 2016; 311: H251-67.
74 Bers DM, Despa S, Bossuyt J. Regulation of Ca2+ and Na+ in normal and failing cardiac myocytes. Annals of the New York Academy of Sciences 2006; 1080: 165-77.
75 Pogwizd SM, Schlotthauer K, Li L, Yuan W, Bers DM. Arrhythmogenesis and contractile dysfunction in heart failure: Roles of sodium-calcium exchange, inward rectifier potassium current, and residual beta-adrenergic responsiveness. Circulation research 2001; 88: 1159-67.
76 Weber CR, Ginsburg KS, Bers DM. Cardiac submembrane [Na+] transients sensed by Na+-Ca2+ exchange current. Circulation research 2003; 92: 950-2.
77 Weber CR, Piacentino V, 3rd, Ginsburg KS, Houser SR, Bers DM. Na(+)-Ca(2+) exchange current and submembrane [Ca(2+)] during the cardiac action potential. Circulation research 2002; 90: 182-9.
78 Szentandrassy N, Birinyi P, Szigeti G, et al. SEA0400 fails to alter the magnitude of intracellular Ca2+ transients and contractions in Langendorff-perfused guinea pig heart. Naunyn-Schmiedeberg's archives of pharmacology 2008; 378: 65-71.
79 Baczko I, Giles WR, Light PE. Resting membrane potential regulates Na(+)-Ca2+ exchange-mediated Ca2+ overload during hypoxia-reoxygenation in rat ventricular myocytes. The Journal of physiology 2003; 550: 889-98.
80 Bourgonje VJ, Vos MA, Ozdemir S, et al. Combined Na(+)/Ca(2+) exchanger and L-type calcium channel block as a potential strategy to suppress arrhythmias and maintain ventricular function. Circulation Arrhythmia and electrophysiology 2013; 6: 371-9.
81 Ozdemir S, Bito V, Holemans P, et al. Pharmacological inhibition of na/ca exchange results in increased cellular Ca2+ load attributable to the predominance of forward mode block. Circulation research 2008; 102: 1398-405.
82 Chen-Izu Y, Ward CW, Stark W, Jr., et al. Phosphorylation of RyR2 and shortening of RyR2 cluster spacing in spontaneously hypertensive rat with heart failure. American journal of physiology Heart and circulatory physiology 2007; 293: H2409-17.
83 Tanaka H, Nishimaru K, Aikawa T, Hirayama W, Tanaka Y, Shigenobu K. Effect of SEA0400, a novel inhibitor of sodium-calcium exchanger, on myocardial ionic currents. British journal of pharmacology 2002; 135: 1096-100.
84 Banyasz T, Magyar J, Szentandrassy N, et al. Action potential clamp fingerprints of K+ currents in canine cardiomyocytes: their role in ventricular repolarization. Acta physiologica (Oxford, England) 2007; 190: 189-98.

85 Wehrens XH, Lehnart SE, Reiken SR, et al. Protection from cardiac arrhythmia through ryanodine receptor-stabilizing protein calstabin2. Science (New York, NY) 2004; 304: 292-6.

86 Choi HS, Eisner DA. The effects of inhibition of the sarcolemmal Ca-ATPase on systolic calcium fluxes and intracellular calcium concentration in rat ventricular myocytes. Pflugers Archiv : European journal of physiology 1999; 437: 966-71.

87 Namekata I, Nakamura H, Shimada H, Tanaka H, Shigenobu K. Cardioprotection without cardiosuppression by SEA0400, a novel inhibitor of Na+-Ca2+ exchanger, during ischemia and reperfusion in guinea-pig myocardium. Life sciences 2005; 77: 312-24.

88 Namekata I, Kawanishi T, Iida-Tanaka N, Tanaka H, Shigenobu K. Quantitative fluorescence measurement of cardiac Na+/Ca2+ exchanger inhibition by kinetic analysis in stably transfected HEK293 cells. Journal of pharmacological sciences 2006; 101: 356-60.

89 Wang J, Zhang Z, Hu Y, et al. SEA0400, a novel Na+/Ca2+ exchanger inhibitor, reduces calcium overload induced by ischemia and reperfusion in mouse ventricular myocytes. Physiological research / Academia Scientiarum Bohemoslovaca 2007; 56: 17-23.

90 Yoshiyama M, Nakamura Y, Omura T, et al. Cardioprotective effect of SEA0400, a selective inhibitor of the Na(+)/Ca(2+) exchanger, on myocardial ischemia-reperfusion injury in rats. Journal of pharmacological sciences 2004; 95: 196-202.

91 Pueyo E, Husti Z, Hornyik T, et al. Mechanisms of ventricular rate adaptation as a predictor of arrhythmic risk. American journal of physiology Heart and circulatory physiology 2010; 298: H1577-87.

92 Satoh H, Ginsburg KS, Qing K, Terada H, Hayashi H, Bers DM. KB-R7943 block of Ca(2+) influx via Na(+)/Ca(2+) exchange does not alter twitches or glycoside inotropy but prevents Ca(2+) overload in rat ventricular myocytes. Circulation 2000; 101: 1441-6.

8. ANNEX

Publications related to the subject of the Thesis